



Investigating size-segregated sources of elemental composition of particulate matter in the South China Sea during the 2011 *Vasco* Cruise

Miguel Ricardo A. Hilario^a, Melliza T. Cruz^b, Maria Obiminda L. Cambaliza^{a,b}, Jeffrey S. Reid^c,
Peng Xian^c, James B. Simpas^{a,b}, Nofel D. Lagrosas^{a, b, *}, Sherdon Niño Y. Uy^b, Steve Cliff^d,
Yongjing Zhao^d

^a Department of Physics, Ateneo de Manila University, Quezon City, Philippines

^b Manila Observatory, Ateneo de Manila University campus, Quezon City, Philippines

^c Marine Meteorology Division, Naval Research Laboratory, Monterey, CA, USA

^d Air Quality Research Center, University of California Davis, CA, USA

Correspondence to: Maria Obiminda L. Cambaliza (mcambaliza@ateneo.edu)

* Now with Center for Environmental Remote Sensing, Chiba University, Japan

Abstract

The South China Sea/West Philippine Sea (SCS/WPS) is a receptor of various natural and anthropogenic aerosol species from throughout greater Asia. In combination with its archipelagic/peninsular terrain and strong Asian monsoon climate, the SCS/WPS hosts one of the most complex aerosol-meteorological systems in the world. However, aside from the well-known biomass burning emissions from Indonesia and Borneo, the current understanding of aerosol sources is limited—especially in remote marine environments. In September 2011, a 2-week research cruise was conducted near Palawan, Philippines to sample the remote SCS/WPS environment. Size-segregated aerosol data was collected using a Davis Rotating-drum Unit size-cut Monitor sampler and analyzed for concentrations of 28 selected elements. Positive Matrix Factorization (PMF) was performed separately on the coarse, fine, and ultrafine size ranges to determine possible sources and their contributions to the total particulate matter mass. Additionally, size distribution plots, time series plots, back trajectories and satellite data were used in interpreting factors. Using tracers of various sources, a linear regression analysis and correlation matrices showed the presence of soil dust and sea spray in the coarse mode, biomass burning in the fine mode and oil combustion in the ultrafine mode. Mass distributions showed elevated aerosol concentrations towards the end of the sampling



28 period which coincided with a shift of air mass back trajectories to Southern Kalimantan. Covariance between coarse and fine
29 mode sources were observed. The PMF analysis resolved five sources across the three size ranges: biomass burning, oil
30 combustion, soil dust, sea spray and a fly ash factor largely composed of heavy metals. The agreement between the PMF and
31 the linear regression analyses suggests the robustness of the PMF solution. While biomass burning is indeed a key source of
32 aerosol, the study shows the presence of other important sources in the SCS/WPS. Understanding these sources is key to
33 characterizing the chemical profile of the SCS/WPS and, by extension, developing our understanding of aerosol-cloud behavior
34 in the region.

35 1. Introduction

36 The South China Sea/West Philippine Sea (SCS/WPS) is a receptor of a multitude of natural and anthropogenic
37 aerosol species. At the same time, due to its archipelagic/peninsular terrain coupled with a strong Asian monsoon climate, the
38 region exhibits some of the world's most complicated meteorology. Together, the SCS/WPS hosts one of the world's most
39 complex and sensitive composition and climate regimes (Balasubramanian et al., 2003; Yusef and Francisco, 2009; Atwood
40 et al., 2013; Reid et al., 2012, 2013, 2015). Particles in the atmosphere are known to influence radiative forcing via absorption
41 and scattering of solar radiation (Nakajima et al., 2007; Boucher et al., 2013; Lin et al., 2013; Ge et al., 2014) and act as cloud
42 condensation nuclei (CCN), affecting cloud reflectivity, evaporation and precipitation rates (Sorooshian et al., 2009; Lee et
43 al., 2012; Boucher et al., 2013; Ross et al., 2018). The northern portion of the SCS/WPS has been known to be impacted by
44 not only China via dust storms (Wang et al., 2011; Atwood et al., 2012) and industrial pollution but also by Southeast Asia
45 through its own anthropogenic pollution and biomass burning (Lin et al., 2007; Cohen et al., 2010a, b; Wang et al., 2011; Reid
46 et al., 2015, 2016). Countries surrounding the Maritime Continent (MC) are known to be impacted by strong seasonal burning
47 (Balasubramanian et al., 2003; Reid et al., 2013). The atmospheric residence times of fine particles allow for long range
48 transport, potentially creating regional and global concerns (Cohen et al., 2010a).

49 Highlighting the unique combination of terrain and sea that feeds into the complexity of the meteorological
50 environment of the region, Reid et al. (2012) and Xian et al. (2013) posed the long-range hypothesis that monsoonal flows and
51 higher-frequency meteorological phenomena are a major factor in seasonal aerosol dispersion. Biomass burning plumes are
52 known to cause severe haze episodes due to these monsoonal flows, raising concentrations of particulate matter (PM) to impact
53 cloud physics and, in some cases, to dangerous air quality levels across large areas, particularly in association with positive
54 phases of the El Niño-Southern Oscillation (ENSO) (Engling et al., 2014; Fujii et al., 2015). Likewise, biomass burning is a
55 significant contributor to the region's CCN budget in all years as are the region's significant anthropogenic emissions
56 (Balasubramanian et al., 2003; Field et al., 2008; Reid et al., 2012; 2013; 2015; 2016; Atwood et al., 2017).

57 Partly due to the emphasis on dramatic biomass burning as the primary source of aerosol particles in the region, the
58 contributions of other regional sources are not well understood or perhaps underappreciated. As the SCS/WPS is host to major
59 population centres, industry, major ports, and coal and oil combustion are expected to be an important regional source of



aerosol particles in the MC. Soil dust and coarse mode biological particles may also play a role in as ice nuclei (O'Sullivan et al., 2014), as biomass burning plumes are known to entrain such particles (Reid et al., 1998; 2005; Schlosser et al., 2017). As such, a network of interacting sources exists in the region surrounding the SCS/WPS, wherein sources mix during transport and complicate source apportionment. Understanding the nature of sources in the remote MC and their contributions is key to characterizing the aerosol environment in the SCS/WPS and its relationship with cloud behavior and precipitation patterns in the region; this is particularly true given the higher sensitivity of clouds to particle perturbations at lower concentrations. However, the identification of sources is complicated by their complex chemistry and interactions with the marine environment (Atwood et al., 2012; 2017).

As part of the Seven South East Asian Studies program (7-SEAS), a research cruise (Reid et al., 2015) was conducted in late September 2011 onboard the Philippine-flagged M/Y *Vasco* in the vicinity of the northern Palawan archipelago. The goal of this cruise was to observe the behavior of aerosol particles in the SCS/WPS and test the transport hypothesis proposed in Reid et al. (2012) that the Philippines is a long-range receptor of aerosol species transported across the SCS/WPS during the boreal summer southwest monsoon from Borneo, Sumatra, and the Malay Peninsula. In particular, the cruise aimed to observe that MC emissions were reaching the Southwest Monsoon monsoonal trough. The Palawan archipelago is a good receptor site for regional emissions due to its largely rural settlements and its location upwind relative to the rest of the Philippines. The sampling period coincided with the passage of one tropical storm and two tropical cyclones (TC). Of particular importance is the passage of a supertyphoon Nesat beginning on 26 September as TC inflow arms are known to cause abrupt changes in regional flows.

As part of the 2011 *Vasco* cruise particulate matter was collected using a size segregated Davis-Rotating Uniform Size-Cut Monitor (DRUM) impactor analyzed for elemental composition. While Reid et al. (2015) noted the presence of plumes in two episodes during the cruise, their initial analysis of the region's atmospheric chemistry also suggested the events were a mix of biomass burning and oil or shipping emissions due to elevated levels of vanadium. Additionally, differences in elemental ratios, mass fractions and back trajectory origins between the two events support the presence of other sources besides biomass burning. From the initial analysis of aerosol chemistry presented by Reid et al. (2015), this study aims to investigate aerosol sources in the SCS/WPS and to further develop the current understanding of the effect of regional meteorological phenomena on aerosol dispersion. The paper shows that, though biomass burning is a major source of aerosols in the SCS, anthropogenic sources such as oil combustion also play an important role in the chemical profile of the region. As we report, soil transport was observed as well.

In this paper we expand on the original 2011 *Vasco* cruise analysis to quantitatively apportion sampled biomass burning and anthropogenic aerosol species. Positive Matrix Factorization (PMF) was performed on size-segregated PM to detect possible size-specific sources (Han et al., 2006; van Pinxteren et al., 2016). Indeed, the relationship between the aerodynamic diameter of a particle and its source has been well-established in literature (Reid et al., 1993; Balasubramanian



et al., 2003; Han et al., 2006; Lestari et al., 2009; Wimolwattanapun et al., 2010; Santoso et al., 2010; Karanisiou et al., 2009; Seneviratne et al., 2010; Atwood et al., 2012; Lin et al., 2015; Cahill et al., 2016). Aerosol factors and characteristics were then used to spawn back trajectories to identify individual island emissions areas.

2. Sampling and Methods

2.1. Overall cruise sampling and environment

A general overview of the 2011 cruise can be found in Reid et al. (2015) and a brief summary is provided here. Sampling was conducted around the Palawan archipelago, an island chain located at the southwestern edge of the Philippines in between the SCS/WPS and the Sulu Sea. Sampling was performed between Manila and the northern tip of Palawan Island onboard the M/Y *Vasco* which left Manila Bay on 17 September 2011 and returned on 30 September 2011 (Fig. 1). Majority of samples were collected around the areas of El Nido and Malampaya Sound (111.1° N, 119.3° E) where the vessel was on station from 21-28 Sept. The largely rural population of Palawan made it an ideal receptor for regional rather than local emissions.



Figure 1. Path taken by the M/Y *Vasco* for 17-20 September (red), 20-28 September (black), 28-30 Sept (blue). Majority of sampling was done at the northern end of Palawan island. Image courtesy of GoogleMaps.

The cruise was conducted at the end of the boreal summer monsoon which usually lasts from June through September (Loo et al., 2014; Chang et al., 2005). The Asian monsoon is caused by the annual march of the sun and asymmetrical heating of air masses due to the complex terrain of Southeast Asia (Chang et al., 2005). The campaign coincided with the peak burning season in Southern Kalimantan and Southern Sumatra, which have been measured to be the highest emitters of biomass burning plumes in the MC (Reid et al., 2012). As the southwest monsoon is characterized by winds travelling southwest to northeast, Reid et al. (2015) proposed that the Philippines was an excellent receptor for regional emissions from the MC.

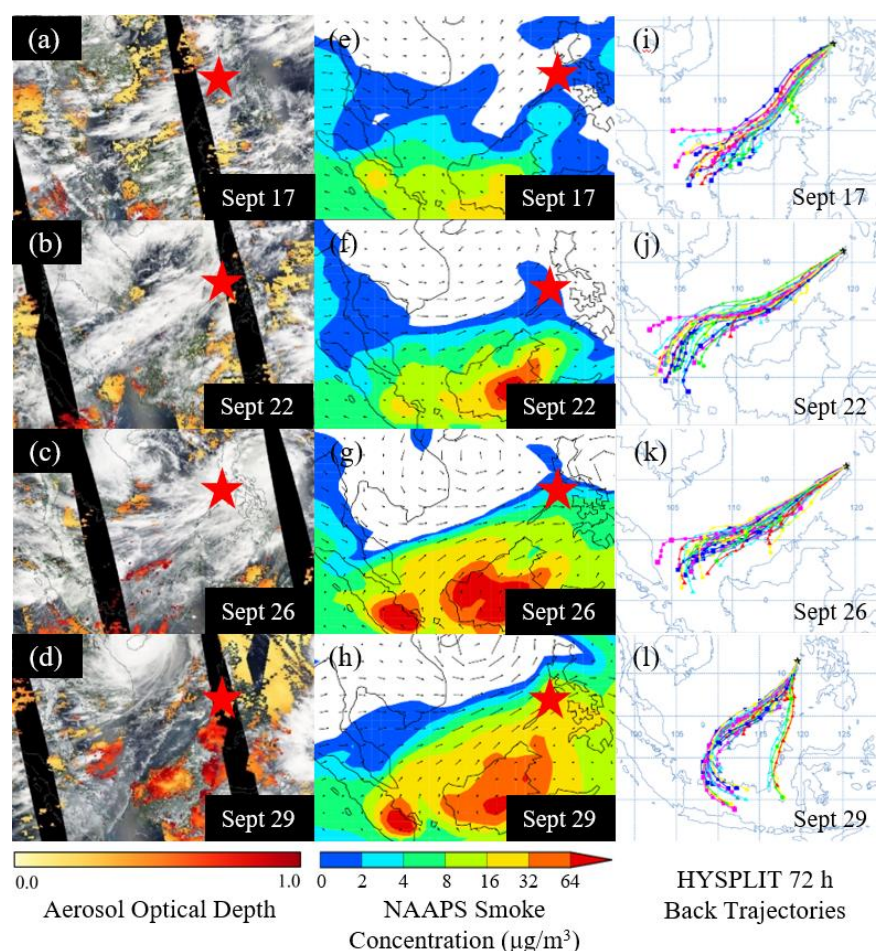
Although 2011 was a moderate La-Niña year, it was noted that fire activity and precipitation levels resembled a neutral year (Reid et al., 2015). The cruise took place when the Madden-Julian Oscillation (MJO) was transitioning from the



115 wet phase to the dry phase, which is expected to enhance burning activity and transport. With the passage of tropical cyclones
 116 (TCs), significant aerosol events were observed to propagate across the region.

117 Reid et al. (2015) described three tropical events that occurred during the cruise, specifically tropical storm (TS)
 118 Haitang, super-TC Nesat, and super-TC Nalgae. The presence of inflow arms in the SCS has been suggested to affect the
 119 aerosol environment by bringing more MC air into the region (Reid et al., 2015). The passage of Nesat was observed to abruptly
 120 affect air mass trajectories coinciding with an enhancement of several elements during the last two days of the cruise.

121 Figure 2 shows the evolution of the meteorological environment over the cruise period with comparisons between
 122 satellite-derived aerosol optical depth (AOD) derived from the MODIS-Terra and MODIS-Aqua satellites, back trajectories
 123 from NOAA Hybrid Single Particle Lagrangian Integrated Trajectory Model (HYSPLIT) and 850 hPa smoke concentrations
 124 from the Navy Aerosol Analysis and Prediction System (NAAPS).



125
 126 **Figure 2.** Satellite images of the SCS/WPS region taken from (a-d) NASA Worldview with overlaid AOD, (e-h)
 127 NAAPS smoke concentration plots ($\mu\text{g}/\text{m}^3$; 850 hPa) and (i-l) HYSPLIT ensemble back trajectories during the cruise



128 (isobaric, 300m AGL, 72 hours, ending at 00:00 UTC/08:00 LST) for 18, 22, 26 and 29 Sept. Red star indicates location
129 of the *Vasco*.

130 2.2. Aerosol sampling and analysis

131 Size-resolved aerosol samples were collected during the cruise using a Davis-Rotating Unit for Monitoring (DRUM)
132 continuously sampling cascade impactor. Samples were collected with a 10 μm inlet and eight size cuts at 5, 2.5, 1.15, 0.75,
133 0.56, 0.34, 0.26, 0.07 μm at a 90-minute time resolution from noontime 17 September until noontime 30 September local-time.
134 Particles were collected on Mylar strips coated with Apiezon grease. The eight drums were rotated at a consistent rate to create
135 a temporal record of mass concentration (Raabe et al., 1988). X-ray fluorescence (XRF) was performed on the DRUM samples
136 at the Advanced Light Source (ALS) of Lawrence Berkeley National Laboratory to measure mass concentrations of 28
137 elements ranging from Na to Pb. In this study, data was filtered based on location notes from the cruise such that samples
138 collected in the vicinity of Manila Bay were excluded from the analysis. Additionally, samples during an 8-hour pump failure
139 that occurred on 20 September were also excluded from the dataset. In the analysis, the stages were aggregated into three
140 modes: coarse (1.15-10 μm), fine (0.34-1.15 μm) and ultrafine (0.07-0.34 μm) modes.

141 2.3. Model and satellite data

142 NOAA Hybrid Single Particle Lagrangian Integrated Trajectory Model (HYSPLIT) back trajectories (Draxler et al.,
143 1998, 1999) were generated throughout the cruise period to investigate locations of aerosol emission. HYSPLIT back
144 trajectories have been used in several studies to establish air mass source regions (Lin et al., 2007; Cohen et al., 2010a; Atwood
145 et al. 2012, 2017). Back trajectories were run for 72 hours for heights of 500 m and 300 m to investigate possible vertical
146 inhomogeneity that has been noted in other SCS/WPS papers (Atwood et al., 2012). Trajectory endpoints corresponded to
147 cruise coordinates. Trajectories were constrained isobarically to limit vertical wind velocity since our area of interest is surface-
148 level emission.

149 The Navy Aerosol Analysis and Prediction System (NAAPS) reanalysis product (Lynch et al., 2016) with driving
150 meteorology was used to provide overall aerosol and meteorological context to the analysis. This reanalysis utilizes a modified
151 version of the NAAPS as its core and assimilates quality controlled retrievals of aerosol optical depth (AOD) from Moderate
152 Resolution Imaging Spectroradiometer (MODIS) on Terra and Aqua and the Multi-angle Imaging SpectroRadiometer (MISR)
153 on Terra (Zhang et al., 2006; Hyer et al., 2011; Shi et al., 2014). NAAPS characterizes anthropogenic and biogenic fine
154 (including sulfate, and primary and secondary organic aerosols), dust, biomass burning smoke and sea salt aerosols. Smoke
155 from biomass burning is derived from near-real time satellite based thermal anomaly data to construct smoke source functions
156 (Reid et al., 2009), with additional orbital corrections on MODIS based emissions and regional tunings. The system has been
157 successfully used to monitor biomass burning plumes and to study the relationship of aerosol lifecycle to weather systems over
158 the MC (Reid et al., 2012, 2015, 2016; Atwood et al., 2013; Xian et al., 2013).



Active fire hotspot data was downloaded from the Fire Information for Resource Management System (FIRMS) (<https://firms.modaps.eosdis.nasa.gov/>). Active fire hotspots and aerosol optical depth (AOD) at a wavelength of 550 nm were tracked throughout the cruise via the Moderate Resolution Imaging Spectroradiometer (MODIS). MODIS detects thermal anomalies across a region to identify possible fire activity. MODIS-derived AOD was used to derive large-scale estimates of PM_{2.5} in some studies (e.g., Zheng et al., 2017). In the study, MODIS was used to track burning emissions which were found to be particularly prevalent in Eastern Malaysia and Indonesia. The use of MODIS to track active fire hotspots has been used in other studies to understand seasonal trends in agricultural burning (Reid et al., 2012) and to identify and locate burning-related sources when used in conjunction with HYSPLIT back trajectories (Atwood et al., 2017).

The NASA Worldview site (www.worldview.nasa.gov), an application operated by the NASA/Goddard Space Flight Center Earth Science Data and Information System (ESDIS) project, was used to supplement the satellite data by providing true color images of the region and is particularly useful in demonstrating sudden changes of cloud environment or monsoon flow caused by tropical cyclones.

2.4. Positive Matrix Factorization

Positive Matrix Factorization (PMF) was used to study the covariability of elemental species. PMF is a multivariate factor analysis technique used in source apportionment that resolves a sample matrix \mathbf{X} ($i \times j$) of i samples and j species into matrices \mathbf{F} ($i \times k$), \mathbf{G} ($k \times j$) and \mathbf{E} ($i \times j$), the source contribution matrix, source profile matrix and residual matrix, respectively, with the assumption of k factors:

$$X_{ij} = G_{ik}F_{kj} + E_{ij}$$

The goal of PMF is to determine the number of factors or sources k such that the solution will be physically interpretable. Developed by Paatero and Tapper (Paatero and Tapper, 1994), PMF is a well-established approach used in previous source apportionment studies (Polissar et al., 1998; Lee et al., 1999; Han et al., 2006; Chan et al., 2008; Karanisiou et al., 2009; Lestari et al., 2009; Santoso et al., 2010; Wimolwattanapun et al., 2010). PMF provides more physically realistic results compared to other factor analysis techniques due to non-negative constraints in the model and better treatment of missing or below detection limit (BDL) values by increasing the associated uncertainty (Paterson et al., 1999).

PMF outputs source profiles (F) and source contributions (G). PMF source profiles were normalized to the percent of species sum, defined as the percent concentration of an element apportioned to a source. A robust mode of PMF was used for analysis, characterized by the parameter α . α is the outlier threshold distance which reduces the effect of extremely large data points and is set at a value of 4.0 to be consistent with other PMF studies (Lee et al., 1999; Han et al., 2006).

For each of the three modes, a minimum Pearson R value of 0.0 was used to filter species based on correlations with the mode-aggregated elemental PM concentration. This means that species negatively correlated with the summed elemental PM



concentration were not included. From the 28 species identified by XRF per DRUM stage, 20 species in the coarse mode, 22 species in the fine mode, and 19 species in the ultrafine mode were used in the size-resolved PMF. Tables S1-3 (Supplementary Information) show the correlation coefficients of the elements, with filtered elements having negative Pearson R values against the summed elemental PM concentration. The filtering of species through correlation was observed to improve the interpretability of the source profiles and remove the need for the matrix rotation parameter, F_{peak} .

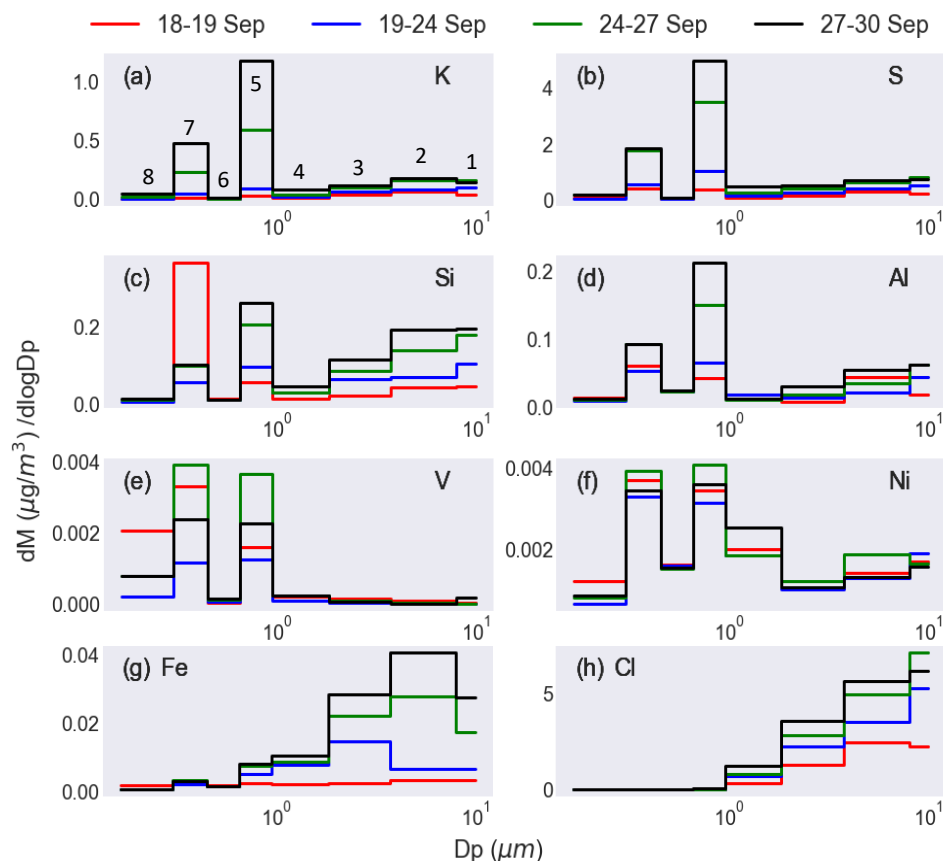
Data screening was performed based on the approach of Polissar et al. (1998) to ensure that no erroneous data points were included in the analysis. Signal-to-noise ratios were determined and species with low ratios (less than 0.2) were excluded from the data set (Paatero and Hopke, 2003). Below detection limit (BDL) values were replaced with half the detection limit (Han et al., 2006). Detection limit values and error values were based on values provided by the Lawrence Berkeley National Laboratory.

The current study employs a size-resolved PMF approach as a supplement to the other analysis methods. PMF is a powerful tool that quantifies the contributions of PM sources and is useful for forming an initial understanding of the possible sources from the data. However, PMF may neglect important events, particularly short-term ones, that can reveal insightful interactions between identified sources and is unable to dissociate covarying sources as it assumes orthogonality between factors (Van Pinxteren et al., 2016).

3. Results I: Mass distributions and time series of selected elements

3.1. DRUM mass distributions

Mass size distributions show normalized species concentrations (dM/dlogDp) across all eight DRUM stages and can be used to validate the signal of a mode-specific tracer. In addition to isolating the signal of a tracer, changes in the mass distributions of key elements over time indicate periods when mode-specific sources are present. Figure 3 depicts the mass size distributions of key elements (a) potassium (K) as a tracer for biomass burning in the fine and ultrafine modes, (b) sulfur (S), which is used as an indicator of combustion, (c) aluminum (Al) and (d) silicon (Si) which are often paired as tracers for soil dust, (e) vanadium (V) and (f) nickel (Ni), which are often paired as tracers of oil combustion, (g) iron (Fe), another key tracer for dust, and (h) chlorine (Cl), a reasonable tracer for sea spray given the sampling location. Figure 3 is further divided into time periods, distinguished by color: 18-19 September (red), 19-24 September (blue), 24-27 September (green) and 27-30 September (black).



215

216 **Figure 3. Time evolution of mass size distributions of key elements over the cruise period. (a) potassium, (b) sulfur, (c)**
 217 **aluminum, (d) silicon, (e) vanadium, (f) nickel, (g) iron, and (h) chlorine. Time periods are colored: 18-19 Sept (red),**
 218 **19-24 Sept (blue), 24-27 Sept (green), 27-30 Sept (black). Stage numbers are depicted in (a).**

219

220 Elements associated with combustion showed generally bimodal distributions with stage 5 (0.56-0.75 μm) and stage 7
 221 (0.26-0.34 μm) peaks. K, S, Al, and Si have very similar mass size distributions over the cruise period which are suggestive of
 222 a common source (Fig. 3a-d). These elements have strong peaks in stage 5 and 7 during the whole cruise but particularly high
 223 values are observed during the last days of the sampling period (27-30 Sept). A general enhancement late in the cruise is likely
 224 related to the increase in the number of active fire hotspots reported by Reid et al. (2015), who attributed these hotspots
 225 primarily to Indonesian Kalimantan and Southern Sumatra. As the cruise took place during the end of the boreal summer, 300
 226 m a.g.l. winds were predominantly southwesterly. A shift in back trajectories at the end of the cruise to the western and southern
 227 coasts of Borneo is observable in Fig. 2l, suggesting the source of the late-cruise enhancement to be the MC, which hosts
 228 elevated aerosol background levels from seasonal burning (Reid et al., 2013). The advection of this large aerosol event can be
 229 observed in the NAAPS smoke model over the region (Fig. 2g, h). The attribution of late-cruise aerosol enhancement to the



MC is in agreement with Reid et al. (2015) who noted that the AOD maps and southwesterly flows towards the end of the cruise were suggestive of southwesterly transport from the MC to SCS/WPS.

Covarying behaviors of Al and Si with K and S suggest possible fine soil entrainment caught in burning updraft (Reid et al., 2015). The stage 5 and stage 7 peaks in S are similar to those observed for northern SCS/WPS in the springtime (Atwood et al., 2012); however, we report enhanced values, attributed to the timing of the sampling period during the MC burning season.

Interestingly, Si shows a strong peak early in the cruise (18-19 Sept) unique to the ultrafine mode which indicates this particular signal may not originate from soil dust but fly ash (Xie et al., 2009). As the *Vasco* was travelling past the islands of Mindoro and Coron en route to Palawan, local sources are likely the cause of the ultrafine Si enhancement. This early-cruise Si signal is further examined through later time series and regressions.

V shows a mass distribution characteristic of a combustion source with strong peaks in stage 5, stage 7, and stage 8 (0.07-0.26 μm) (Fig. 3e). Almost no contribution was observed for coarser stages 1 through 4 (0.75 -10 μm), indicating that V did not originate from soil (Lin et al., 2015) and can be treated as a tracer for oil combustion. Ni shows a similar bimodal mass distribution (Fig. 3f) but had a larger spread over the eight stages than V, which may be due to contributions from other sources such as fly ash (Davison et al., 1974).

Fe and Cl, well-known tracers for soil dust and sea spray, respectively, showed coarse-mode distributions that taper off considerably in the submicron stages (Fig. 3g, h). Cl shows a purely coarse distribution which suggests sea spray considering the sample location (Viana et al., 2008; Gugamsetty et al., 2012; Farao et al., 2014). Fe shows small peaks in stage 4 (0.75-1.15 μm), stage 5, and stage 7; however, these do not constitute a significant signal relative to its coarse mode concentrations. As such, we treat Fe as our coarse mode soil dust tracer. The mass distribution of Fe is observed to increase across stages 1 through 3 (2.5-10 μm) over the cruise period. The increase in coarse Fe coincides with the NAAPS-simulated transport of smoke (Fig. 2g, h) and mirrors the enhancements of K, S, Si (Fig. 4a, b), and Al (Fig. S1a, b). These patterns suggest that coarse soil dust accompanies smoke emissions, possibly through entrainment. The presence of soil dust is further corroborated by Fig. 3c and Fig. 3d, which show the presence of Al and Si in the coarse mode. The distinct coarse and fine mode peaks of Al and Si indicate separate soil dust sources. As fine mode particles have longer residence times (Cohen et al., 2010a), the fine peaks may be an indicator of long-range transport of fine soil dust through the SCS/WPS.

Interpreting DRUM data reveals insights about the composition and interpretation of sources. Table 1 shows the ratios of elemental $\text{PM}_{1.15}/\text{PM}_{10}$ mass concentrations. As in Atwood et al. (2012), the ratio-slope was computed by taking the slope of the linear regression line between $\text{PM}_{1.15}$ and PM_{10} mass concentrations, accompanied by r^2 values. Direct averages of per-timestamp ratios of $\text{PM}_{1.15}$ and PM_{10} were also taken to compute for ratio-averages, accompanied by the standard deviation of the ratios. Fe and Cl both had ratios of 0.06, which confirm the predominantly coarse nature of these species. As commonly



used tracers of soil dust, Al and Si show moderate ratio-slope values of 0.51 and 0.29, respectively, suggesting that Al resides in both coarse and fine ($PM_{1.15}$) modes while Si is predominantly coarse. As expected, elements commonly associated with anthropogenic species such as V, K, and S show high $PM_{1.15}/PM_{10}$ ratios (0.8 and above) which indicate that these elemental particles largely reside in the fine and ultrafine modes. The high ratios of V, K, and S provide evidence for the presence of anthropogenic emissions from sources such as oil combustion and biomass burning while the low ratios of Fe and Cl support their treatment as tracers for soil dust and sea spray, respectively.

The time-resolved DRUM data is important for showing variations in species which may be representative of important aerosol events. Thus, observations on the time-resolved DRUM data can aid in our analysis. At the beginning of the cruise, between 18 to 19 Sept, V, Ni, and Si show enhancements in stages 5, 7, and 8. The stage 7 Si peak during this time is the maximum concentration over the entire cruise period, so this warrants further analysis through later time series and regressions. The period of 19–24 Sept shows a low point in the DRUM peaks of several elements, most notably combustion tracers K and V (Fig. 3a, c), while Cl (Fig. 3h) shows higher peaks in the coarse-mode which suggests a period of clean marine aerosol. This period was described by Reid et al. (2015) as the cleanest of the cruise. The NAAPS model shows nearly zero smoke concentration at the sampling site (Fig. 2f) while 72-h HYSPLIT back trajectories indicate that air masses originate from central SCS/WPS (Fig. 2j). From 24 to 27 Sept, we observed the first major aerosol event characterized by the stage 5 and 7 enhancements of several combustion elements: K, S, Al, Si, V, and Ni (Fig. 3a–f). Fe, our coarse-mode soil dust tracer, shows enhancements in stages 1 to 3 (Fig. 3g), which points to combustion-related entrainment of soil dust in the coarse mode. The NAAPS model (Fig. 2g) depicts the intensification and spread of a smoke-related aerosol event that had been escalating in southern Kalimantan since 22 Sept, reaching the *Vasco* around 26 Sept. During this mid-cruise period, concentrations of biomass burning species K, S, Si, Al are elevated, and oil combustion tracers V and Ni show their maximum concentrations for the cruise in stages 5 and 7 (Fig. 4e, f). The last period, 28 to 30 Sept, depicts the highest concentrations of elements associated with biomass burning (Fig. 4a, b; Fig. S1a, b). As seen in the NAAPS smoke model (Fig. 2h) and HYSPLIT model (Fig. 2l), the westward movement of TC Nesat across the region alters back trajectories to wind around Borneo island, reaching southern Kalimantan which hosted a high active fire hotspot density during the time (Reid et al., 2015), thus bringing polluted air masses toward the sampling site. Stage 5 and 7 peaks of K and S are quite notable as no other stages show significant enhancements in response to this event. Fe, Al, and Si show similar changes but for the coarser stages 1 to 3 (Fig. 3g), indicating a covariance of soil dust and biomass burning tracers. The temporal trends from the DRUM data serve as an entry point into the time series analysis. By identifying key DRUM stages and time periods per element based on their mass size distributions, we can then examine these stages to observe aerosol events over the cruise period.

3.2. Time series of selected elements

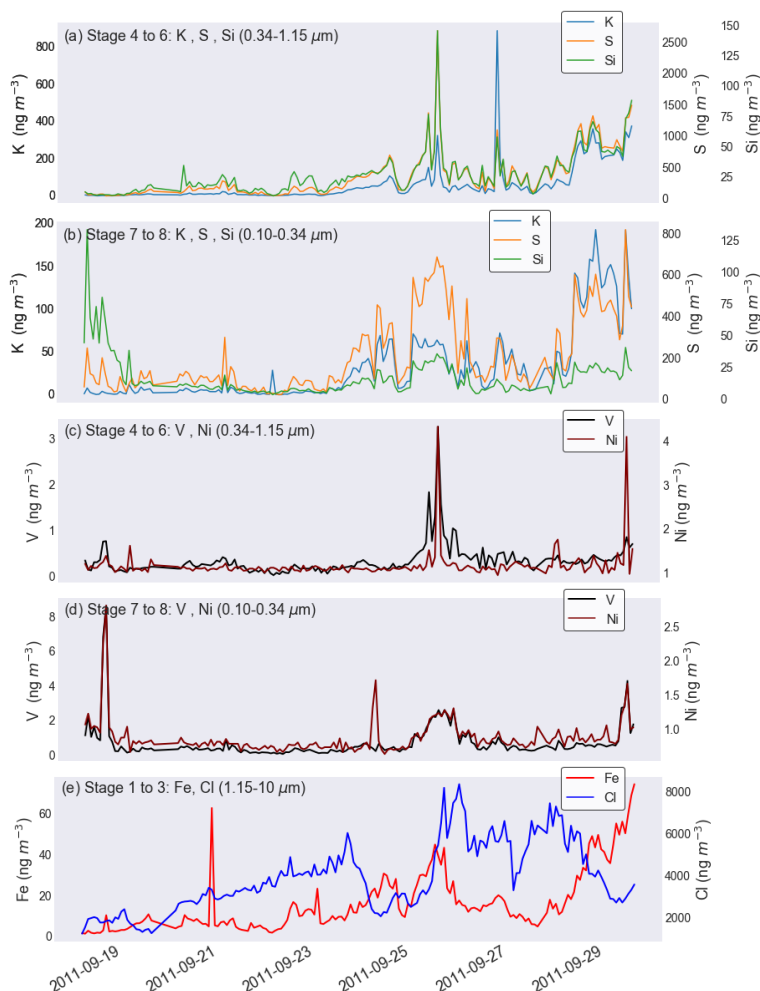


Figure 4. Time series of (a) Stage 4-6 K, S, Si, (b) Stage 7-8 K, S, Si, (c) Stage 4-6 V, Ni, (d) Stage 7-8 V, Ni, and (e) Stage 1-3 Fe, Cl.

The first few days of the cruise showed an 18 Sept event in oil combustion tracers V and Ni in the ultrafine mode (Fig. 4d) with a coincident but lower-magnitude response in the fine mode (Fig. 4c). Ultrafine mode V and Ni show their maxima for the cruise period during this time, expanded further in Section 5. High concentrations of ultrafine Si were sampled during this time from the beginning of the cruise until 19 Sept when it dropped to stable background levels. This early-cruise enhancement was also seen in its mass distribution plot (Fig. 3c). As the *Vasco* was traveling among islands, the Si signal may be due to local sources en route to the El Nido sampling site.

Reid et al. (2015) noted periods of clean regime after departing Manila Bay through midday 22 Sept, observable in the consistently low concentrations of various elements (Fig. 4). Chlorine shows a gradual increase in concentration from 20 Sept until 24 Sept. Chlorine, although it ages into HCl, is assumed to be fresh due to the sampling location and can therefore be used as an indicator of sea spray. Interestingly, coarse-mode Cl (Fig. 4e) showed peak concentration times during low points



in the concentrations of anthropogenic aerosol species (Fig. 4a-d), marking periods of clean marine aerosol on 22-24 Sept and 26-28 Sept, likely through wet deposition processes. During these times, back trajectories shift away from source regions and traverse open sea (Fig. 2j, k) which also hosts a lower shipping route density compared to coastal regions (Fig. S2, Supplementary Information). The first half of the cruise also saw the lowest concentrations from species associated with biomass burning, specifically submicron K, S, Si, (Fig. 4a, b), and Al (Fig. S1a, b, Supplementary Information). These species track each other quite well throughout the cruise period indicating a common source.

The event between 24 Sept and 26 Sept is observable on the time series of several key elements. The plume was the first of two distinct plume events reported by Reid et al. (2015) with the later plume occurring on 29 Sept. The enhancement of all elements in Fig. 4 suggests a mix of biomass burning, oil combustion and soil dust influences within the 24-26 Sept plume. Fine mode V and Ni show their maximum concentrations for the cruise during this event (Fig. 4c). Although these two plumes appeared as one uniform progression across the SCS/WPS region on the NAAPS smoke model (Fig. 2h), the time series showed the presence of two distinct events (Fig. 4), which is corroborated by observations from Reid et al. (2015). During this period, plume concentration dropped sharply before recovering due to the passage of squall lines sharp, observed in the time series for K, S, Si, Fe, and Cl (Fig. 4a, b, e). As concluded in Reid et al. (2015), frequent, short-term events such as this must be accounted for in studies on aerosol-convection interaction.

The period between plumes (26-28 Sept) is characterized by an overall drop in the aerosol concentration of species associated with anthropogenic sources (K, S, V, Ni; Fig. 4a-d). As Cl concentrations show peak values during this period (Fig. 4d), this indicates a period of pure marine aerosol sampling similar to the 22-24 Sept clean period. Coinciding with the passage of TC Nesat through the SCS/WPS, the observed drop in aerosol concentration is attributed to a possible restriction of shipping traffic in response to the TC and scavenging of aerosols by precipitation along the TC inflow arm (Fig. 2c) (Reid et al., 2015).

The last days of the cruise were particularly eventful as the largest aerosol event of the cruise period was visible on the NAAPS model in the form of smoke (Fig. 2h), accompanied by the spread of high AOD values throughout the SCS/WPS (Fig. 2d). Although the large areas of cloud cover created by TC Nesat hinders the detection of AOD on 26 Sept, the region is free of cloud cover by 29 Sept that significant AOD values were observed to visibly stretch from Southern Kalimantan towards the Vasco sampling site (Fig. 2d). In general, the NAAPS smoke transport model agrees with the spatial distribution of high AOD. Here, NAAPS modelling of smoke transport is useful in demonstrating the event's northward advection and the severity of smoke concentration in Borneo island on 26 Sept (Fig. 2h). Time series plots of elements associated with biomass burning (K, S, Si; Fig. 4a, b) and coarse mode soil dust (Fe; Fig. 4d) show significant enhancements during this time which were also observed on their mass distributions (Fig. 3). HYSPLIT back trajectories show that air masses originate from Southern Kalimantan during this period as opposed to mainland Malaysia during the first half (Fig. 2j, l). The shift in air mass trajectories is attributed to the passage of TC Nesat through the region as inflow arms from TCs have been observed to accelerate air mass



advection across the SCS/WPS, bringing more MC air into the region (Reid et al., 2012; 2015). The observed transport of emissions from Borneo indicates that TC-enhanced long-range transport is a significant factor in SCS/WPS aerosol dispersion.

4. Results II: positive matrix factorization and regressions

4.1. Source apportionment via positive matrix factorization

To verify groupings of key elements and aid in source identification, size-resolved PMF was performed. As described in Section 2, the eight-stage DRUM data were combined into coarse (1.15-10 μm), fine (0.34-1.15 μm) and ultrafine (0.07-0.34 μm) modes and the species included in the PMF analysis were then filtered based on their correlation to the aggregated PM concentration. The PMF analysis resolved five sources across the three size ranges: biomass burning, oil combustion, soil dust, sea spray and fly ash (Table 2).

Figure 5 shows the percent contribution of each source relative to the total elemental PM mass. One strength of PMF is its quantification of a source's contribution. As expected, natural sources such as the crustal source/sea spray and soil dust mainly contribute to the coarse mode while combustion-related sources such as biomass burning and oil combustion exist in the fine and ultrafine modes. The existence of these sources in their expected modes is an indicator of the successful implementation of PMF. The following sections describe the observed characteristics of sources determined by PMF.

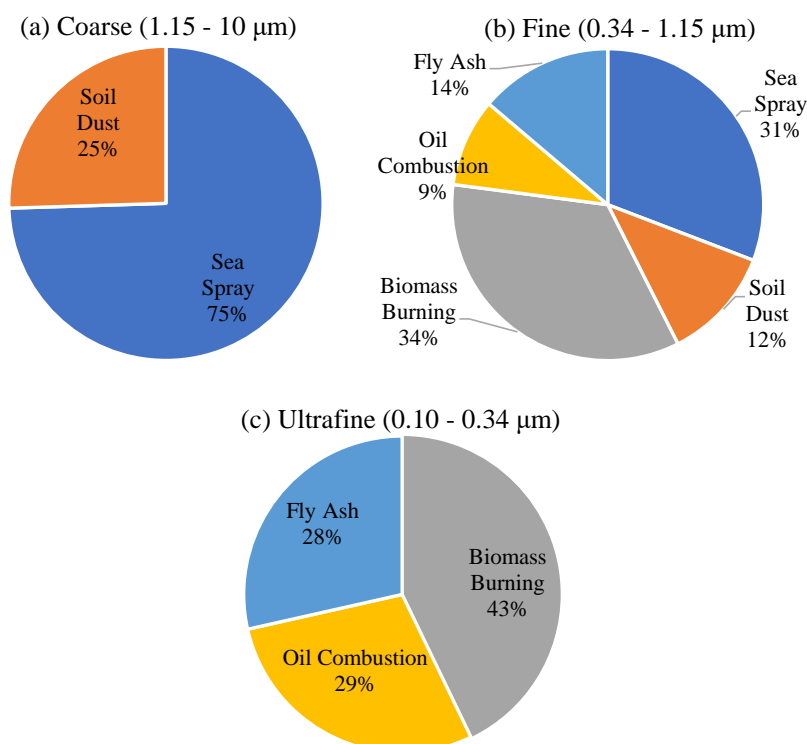
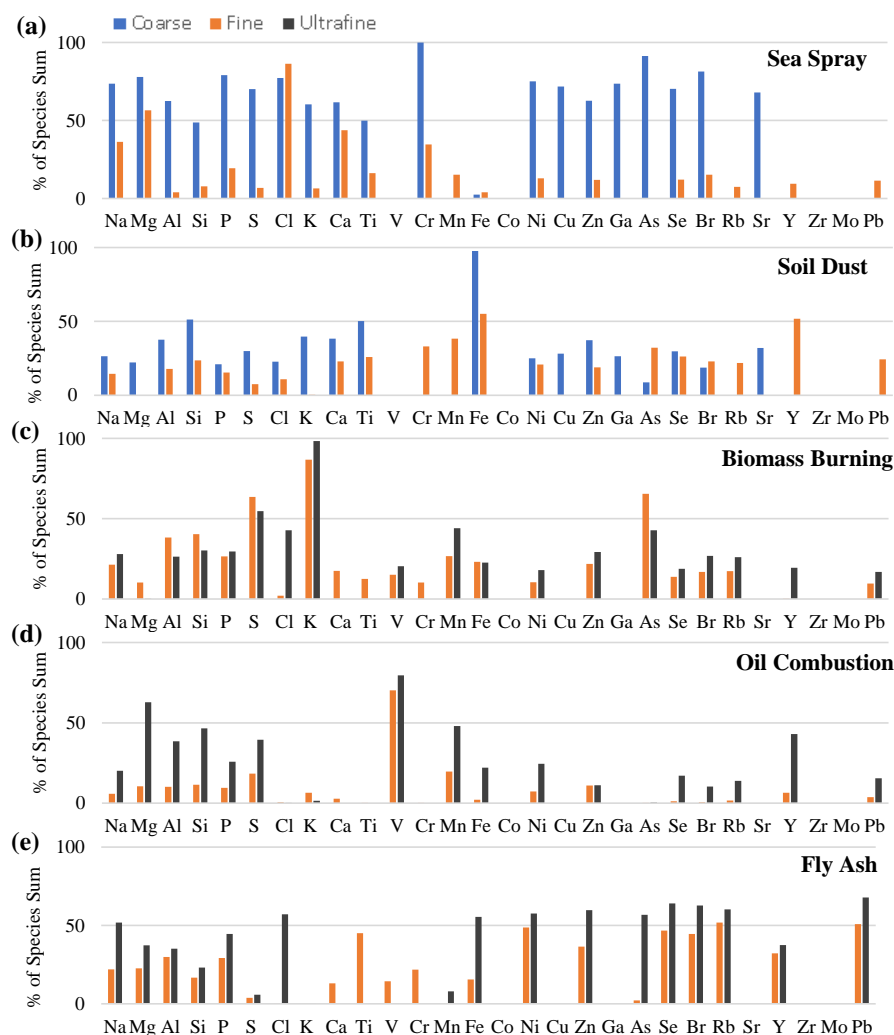


Figure 5. Contributions of factors to the total elemental PM mass.



352



353

354 **Figure 6.** PMF source profiles across different size ranges displayed by percent of species sum for (a) sea spray, (b) soil
 355 dust, (c) biomass burning, (d) oil combustion, and (e) fly ash. Coarse: Stage 1-3 (1.15-10 μm ; blue), Fine: Stage 4-6
 356 (0.34-1.15 μm ; orange), Ultrafine: Stage 7-8 (0.07-0.34 μm ; black).

357 **Sea spray:** This factor was resolved in the coarse and fine modes characterized by strong apportionments for Na, Mg,
 358 Cl, P, and S in the coarse mode, and Cl and Mg in the fine mode as shown in the source profile of Fig. 6a. These elements are
 359 indicative of sea spray (Han et al., 2006; Wang et al., 2014). Cl has been treated as a sea spray tracer under the assumption
 360 that the sampled Cl originated from freshly produced sea spray (Atwood et al., 2012). This is likely the case for the cruise as
 361 sampling was done over sea water. The factor showed quite high mass contributions to the coarse (75%) and fine (31%) modes,
 362 attributed to the sampling location over water (Fig. 5a, b).

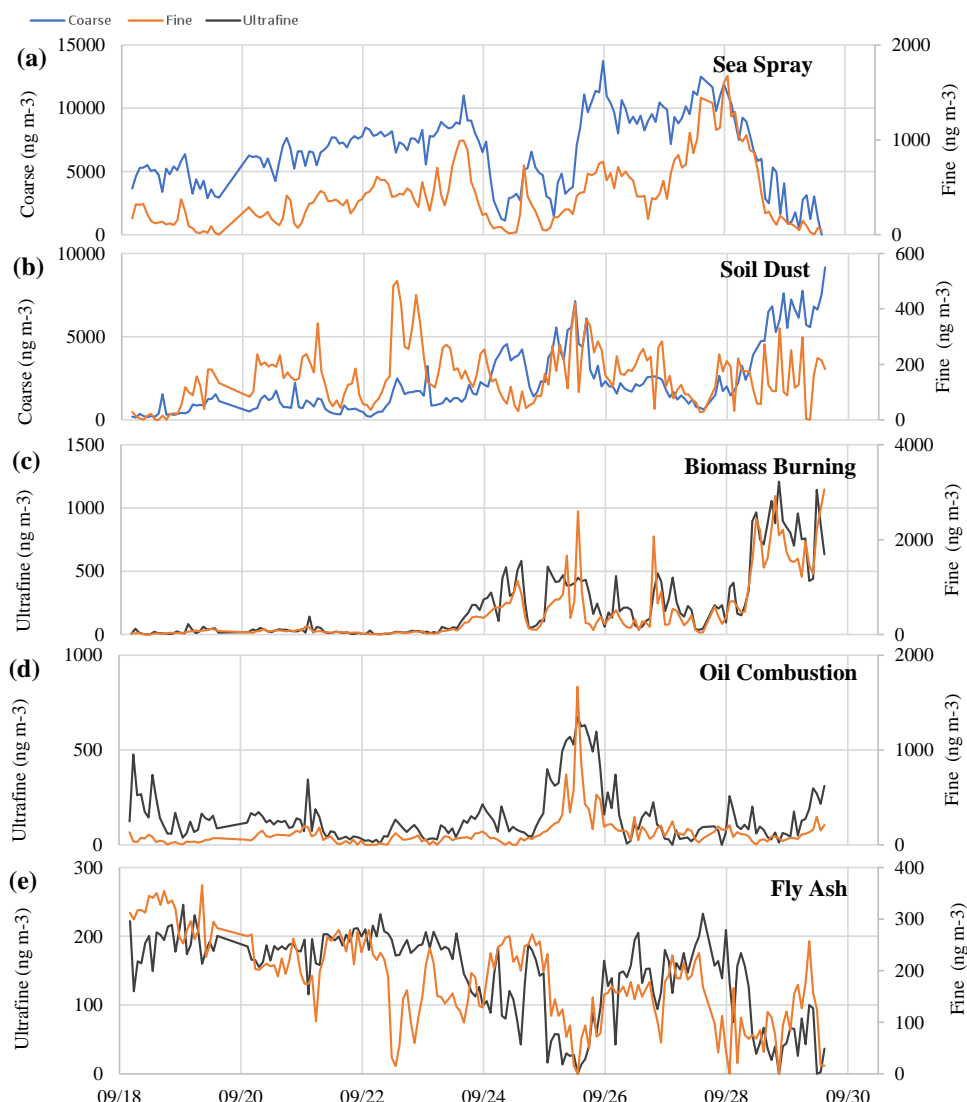


363 **Soil dust:** This factor was characterized by the presence of Fe, Al, Si, K, Ca, Ti, and Zn in the coarse mode and Fe, Cr,
364 Mn, and Y in the fine mode (Fig. 6b; Table 2). Several of these elements are associated with soil dust (Artaxo et al., 1990,
365 1998; Lestari et al., 2009; Wimolwattanapun et al., 2010; Gugamsetty et al., 2012). Soil dust may originate from the nearby
366 island of Palawan but also can potentially come from Borneo. The PMF model was able to distinguish between the sea spray
367 and soil dust factors. As sea spray aerosol is assumed to be freshly sampled during the cruise and the temporal trends of the
368 two sources are distinct (Fig. 7a, b), this suggests the possibility of a long-range transport mechanism for coarse mode soil
369 dust. Fe serves as our tracer for soil dust due to its high apportionment in both soil dust modes. This factor showed mass
370 contributions of 25% and 12% in the coarse and fine modes, respectively, which indicates the predominantly coarse mode
371 contribution of the factor (Fig. 5a, b).

372 **Biomass burning:** This factor was characterized by high levels of K and S, and moderate levels of Al, As, and Si which
373 were found to be associated with biomass burning in previous studies (Artaxo et al., 1998; Han et al., 2006; Lestari et al., 2009;
374 Atwood et al., 2012; Alam et al., 2014) (Fig. 6c; Table 2). The factor showed the highest percent contributions to the PM mass:
375 34% and 43% in the fine and ultrafine modes, respectively. The sources of the 26 Sept and 28-30 Sept events (Fig. 7c) will be
376 investigated in Section 5. The presence of crustal elements Fe, Si, and Al in the source profile and the covariance of the coarse
377 soil dust factor (Fig. 7b) with this factor (Fig. 7c) indicate possible soil dust entrainment during burning updraft (Reid et al.,
378 2015; Schlosser et al., 2017).



379



380 **Figure 7. PMF source contributions across size ranges displayed concentration (ng/m³) for (a) sea spray/crustal source,**
 381 **(b) soil dust, (c) biomass burning, (d) oil combustion, and (e) fly ash.**

382 **Oil combustion:** This factor was characterized by high levels of V (Fig. 7d; Table 2), a well-documented tracer for oil
 383 combustion (Hedberg et al., 2005; Mazzei et al., 2008; Becagli et al., 2012). As shown in Fig. 5, the oil combustion factor only
 384 appeared in the fine and ultrafine sizes, contributing 9% and 29%, respectively, to the total elemental PM mass. The increasing
 385 contribution towards finer stages corroborates the identification of the factor as an anthropogenic source. The presence of oil
 386 combustion is expected as the SCS/WPS hosts high shipping volume, particularly in parts of the Borneo coast (Fig. S2).

387 **Fly ash:** This factor was observed in the fine and ultrafine modes, characterized by high levels of trace metals Ti, Ni, Zn,
 388 Se, Br, Rb, Y, and Pb in the fine mode; Fe, Ni, Zn, As, Se, Br, Rb, and Pb in the ultrafine mode (Fig. 6e); and a source

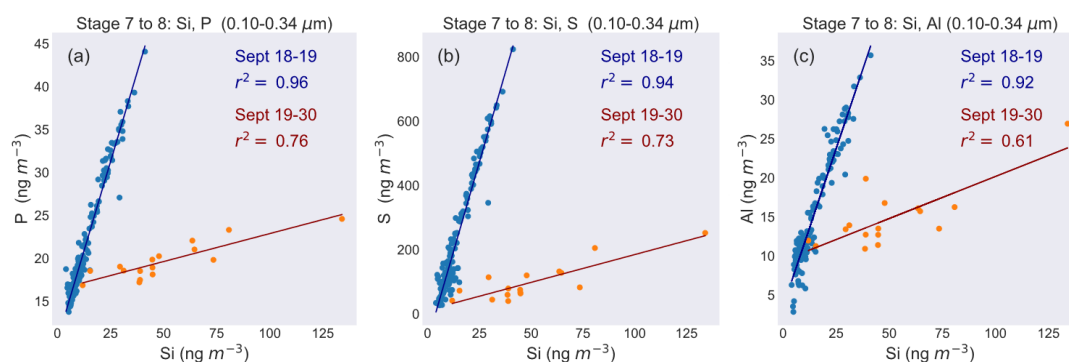


contribution without distinct events (Fig. 7e). The presence of As, Se, Zn, and Ni are indicative of fly ash (Davison et al., 1974; Markowski et al., 1985; Deonarine et al., 2015). The source contribution time series shows a background-type signal. The factor contributed 14% and 28% to the total elemental PM mass for the fine and ultrafine size ranges, respectively (Fig. 5), which is indicative of a combustion-type source. Long-range transport of fly ash from coal-fired power plants in Indonesia or mainland Malaysia may be responsible for the appearance of the factor as no local coal-fired power plants could be found upwind of the sampling site in 2011.

The PMF analysis resolved the presence of five sources across the ultrafine, fine and coarse modes which aids in directing further analysis by identifying key species in the source profiles. Pearson correlation heatmaps (Fig. S3-5, Supplementary Information) and matrices (Tables S1-S3, Supplementary Information) were constructed to examine the relationships between species. The first column of the correlation outputs (Fig. S3-5, Tables S1-S3, Supplementary Information) shows the correlation coefficient of the element when compared to the summed elemental PM for that mode. Similar groupings of elements were observed when compared to the PMF source profiles, indicating the robustness of the analysis. In the coarse mode (Fig. S3; Table S1, Supplementary Information), we observe high correlations between Na, Mg, Cl, P, S, K, Ca, Br, and Sr, which are associated with sea spray (Han et al., 2006; Wang et al., 2014). Fe, Ti, Mn, Si, and Zn show moderate to high correlations in the coarse mode, indicative of dust (Karanisiou et al., 2009; Wimolwattanapun et al., 2010; Lin et al., 2015; Landis et al., 2017). In the fine mode, moderate to high correlations between Al, Si, P, S, K, Br are observed (Fig. S4, Table S2, Supplementary Information). Several of these biomass burning elements show similarly strong correlations in the ultrafine mode (Fig. S5, Table S3, Supplementary Information). V and Ni show a high correlation coefficient (0.91) in the ultrafine mode, indicative of oil combustion. The excellent correspondence between the observed groupings of elements based on correlation (Tables S2-4, Supplementary Information) and the sources resolved by PMF (Table 2) adds confidence to the identification of key sources during the cruise. However, as PMF is an unsupervised technique, it may miss significant aerosol events, particularly transient ones. To further expand on the relationships between elements, we turn to regression analysis.

4.2. Regressions of selected elements

An early-cruise ultrafine Si event was shown in the mass size distribution (Fig. 3d) and the time series (Fig. 4b) of ultrafine Si. Fly ash was the hypothesized source of the ultrafine Si signal; however, although the PMF analysis showed the presence of fly ash, Si was not attributed significantly to the fly ash factor (Fig. 6e). Additionally, none of the factor contributions from PMF showed a similar trend between 18-19 Sept as ultrafine Si. Regressions show that, between 18 and 19 Sept, Si had distinct ratio slopes and the highest correlations with P ($r^2 = 0.76$), S ($r^2 = 0.73$), and Al ($r^2 = 0.61$) (Fig. 8; Table S4) but showed poor correlations with other fly ash elements (As, Se, Pb; $r^2 < 0.12$). As it was early in the cruise, the *Vasco* was travelling past nearby islands en route to Palawan. Therefore, local sources en route to Palawan may be the source of the ultrafine Si enhancement.



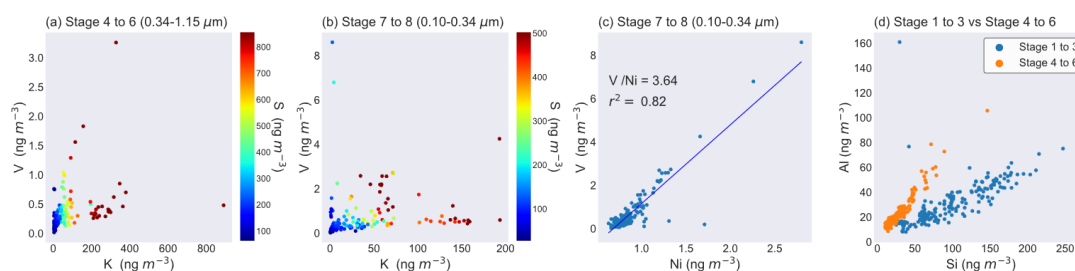
420

421 **Figure 8. Linear regressions of ultrafine Si and its most highly correlated elements (a) P, (b) S, (c) Al, divided by**
 422 **cruise period before Sept 19 (red) and after Sept 19 (blue).**

423 As S is an indicator of general combustion (Atwood et al., 2012), it is important to elucidate its relationship with
 424 tracers of other combustion sources. Fine mode and ultrafine mode linear regressions of K and V, colored by the raw
 425 concentration of S at each timestamp, were taken to show the relationships between the three species (Fig. 9a, b). S is seen to
 426 covary more with K than V as seen with the clearer color gradient following the K-axis, suggesting the origin of S during the
 427 cruise to be more dominantly from biomass burning rather than oil combustion. Multiple linear regression was also performed
 428 for these elements on the fine and ultrafine modes (Fig. S6, Supplementary Information). It was found that K and V were
 429 excellent predictors of S for most of the cruise but the model required the addition of Al to capture the variance in S between
 430 24 and 26 Sept. A detailed description of the multiple linear regression analysis can be found in the Supplementary.

431 The ratio between V and Ni is often used as an indicator of the type of oil combustion source (Hedberg et al., 2005;
 432 Nigam et al., 2006; Mazzei et al., 2008; Becagli et al., 2012; Lin et al., 2015). Linear regression plots of V and Ni have a slope
 433 of 3.64 in the ultrafine mode (Fig. 9c). Nigam et al. (2006) measured a V/Ni ratio of 3.5-4 when sampling shipping emissions
 434 directly from the exhausts of various ship engines which suggests shipping to be the main source of ultrafine mode oil
 435 combustion during the cruise.

436 As soil composition varies geographically, soil dust ratios are excellent indicators of a plume's origin (Prospero et
 437 al., 1999; Song et al., 2006; Witt et al., 2006). Figure 9d shows linear regressions of soil dust elements in the coarse and fine
 438 modes. Al and Si, well-known indicators of dust (Viana et al., 2008; Tian et al., 2016; Landis et al., 2017), show moderate
 439 correlations with each other in the coarse and fine modes but slightly differ in ratio-slopes between the fine (Si/Al ~ 1.3; r² =
 440 0.94) and coarse (Si/Al ~ 0.93; r² = 0.78) modes (Fig. 9d). This indicates a source of fine mode soil dust source enriched in Si;
 441 however, this could also be a matrix effect from the XRF analysis. As the *Vasco* remained near Palawan island, local dust
 442 could be the source of coarse-mode Si-enrichment; however, soil dust from Borneo is also a possibility.



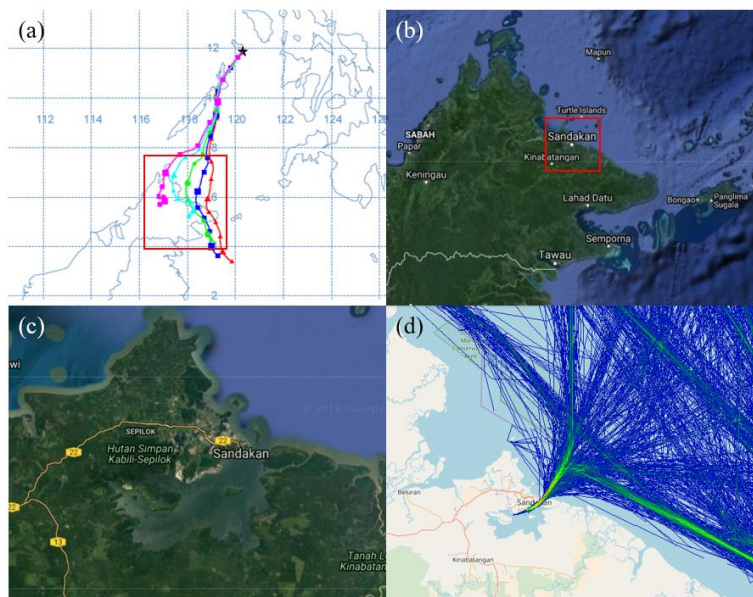
443

444 **Figure 9.** Scatter plot of key species during the cruise. (a) fine mode K, V colored by the raw concentrations of S per
 445 timestamp, (b) ultrafine mode K, V likewise colored by raw concentrations of S per timestamp, (c) ultrafine mode V,
 446 Ni, and (d) coarse and fine mode Al, Si.

447 5. Results III: Back trajectory analysis

448 18-19 Sept: Ultrafine V, Ni enhancement from Sandakan, Sabah

449 As described in Section 3, ultrafine mode V and Ni show a maximum around 18 Sept (Fig. 4d). As the *Vasco* was traveling
 450 near local islands, the event may originate from a local source; however, back trajectories propose an oil combustion source
 451 in Borneo. Back trajectories were generated every hour between 14:00 to 18:00 UTC (corresponding to 22:00 to 02:00 LST)
 452 on 18 September and show a westward shift along the eastern coast of Borneo (Fig. 10a). The coast of Borneo is largely forest
 453 (Fig. 10b) but hosts the city of Sandakan, one of Sabah's major ports (Fig. 10c, d). In addition to shipping traffic (Fig. 10d),
 454 Sandakan contains oil depots which are a major source of industry in the area. During the westward shift of the back
 455 trajectories, air masses pass through Sandakan at around 16:00 UTC, approximately the time of the sampled spike in V. The
 456 shipping activity and oil depots present in this area may be responsible for the spike in oil combustion tracers, indicating the
 457 complexity of aerosol transport in the region as small cities like Sandakan may be a source of significant spikes in aerosol.



458
 459 **Figure 10. Determination of 18 September event using (a) HYSPLIT back trajectories, (b, c) Google Maps view of the**
 460 **northeastern coast of Borneo, (d) Density of shipping traffic from Sandakan, Sabah (source: MarineTraffic). Red**
 461 **squares indicate the location of the succeeding plot.**

462 **20-24 Sept: Clean marine period**

463 The first half of the cruise showed the lowest concentrations of elements associated with biomass burning K, S, Si, and
 464 Al. Back trajectories during this early period originate from the northern part of Borneo and do not penetrate deeply into the
 465 MC until late into the cruise (Fig. 2l). During this period, HYSPLIT back trajectories show that air mass pathways shift away
 466 from the Borneo coasts towards open sea (Fig. 2j). In addition to the shift away from biomass burning sites, back trajectories
 467 between 22 and 24 Sept pass through areas of open sea that host lower levels of shipping traffic (Fig. S2, Supplementary
 468 Information).

469 **24-26 Sept: Large mixed aerosol event from northwest Borneo**

470 Around 26 Sept, increases in fine mode V and Ni occurred when air masses passed through the northwest coast of Borneo,
 471 suggesting the presence of ports or oil depots like with the aforementioned spike on 18 Sept from Sandakan. Back trajectories
 472 generated every 6 hours starting from 24 Sept 15:00 UTC until 26 Sept 09:00 UTC show little change over this period (not
 473 shown) and intersect with the shipping route hub located along northwest Borneo which would explain the V and Ni spikes
 474 (Fig. 2k, S1, Supplementary Information). The enrichments of biomass burning and combustion tracers K and S in the sampled
 475 air mass span a wider period beginning on 24 Sept until 26 Sept. This may be due to burning activity along the coast of Borneo
 476 which hosts several MODIS-detected active fire hotspots. Late-night land breeze from the island may have advected polluted
 477 air masses towards the coast.



478 **28-30 Sept: Large biomass burning event from Southern Kalimantan**

479 Enhancements of these elements after 28 Sept coincide with a regional increase in AOD (Fig. 2d) and are captured by
480 the NAAPS model in the form of a large smoke event advected northeast (Fig. 2h). Linear regressions show this large aerosol
481 event at the end of the cruise as a distinct group of points with enhanced concentrations of K and S (Fig. S7, Supplementary
482 Information), suggesting an increase in biomass burning activity during this time. Reid et al. (2015) observed a sharp increase
483 in the number of active fire hotspots, particularly in Sumatra and Southern Kalimantan. As discussed prior and depicted in Fig.
484 2, TC Nesat played a major role in synoptic wind patterns during the cruise, causing a shift in back trajectories after 28 Sept
485 to the southwest coast of Borneo island. Thus, the enhancements of submicron K, S, Si and Al likely originate from biomass
486 burning in the MC.

487 **6. Summary and conclusions**

488 This study describes the size-resolved aerosol elemental composition of particles collected by a DRUM rotating impactor
489 during the 17 to 30 September 2011 M/Y *Vasco* cruise in the vicinity of the Palawan island of the Philippines. This region was
490 chosen due to its location as a receptor for MC aerosol sources, such as biomass burning, oil combustion and soil dust.
491 Meteorological conditions during the cruise were conducive to southwesterly long range transport for seasonal burning aerosol
492 which was observed in the concentration time series of tracers and satellite-derived AOD. Size-resolved aerosol composition
493 in the coarse (1.15-10 μm), fine (0.34- 1.15 μm) and ultrafine (0.07-0.34 μm) modes were used as key tracers to ascertain
494 source contributions. Despite the meteorological complexity of the SCS/WPS, we can gain insights into aerosol sources by
495 focusing on key elemental species. The time series of key elements showed distinct events on 18-19 Sept, 24-26 Sept, and 28-
496 30 Sept, with clean aerosol periods between events. These aerosol events served as case studies of sources in the region. While
497 biomass burning is indeed a key source of aerosol, other sources such as oil combustion, sea spray, fly ash, and soil dust
498 contribute to the chemical profile of the SCS/WPS during the southwest monsoon. Understanding these sources is key to
499 characterizing aerosol composition and transport in the SCS/WPS and, by extension, developing our understanding of aerosol-
500 cloud behavior in the region. As back trajectory analysis and aerosol chemistry showed the presence of multiple key sources,
501 the general conclusions of the study show that:

- 502 1. Mass distributions of key elements showed the evolution of aerosol chemistry throughout the cruise and
503 interesting covariances between modes. Stage 5 (0.56-0.75 μm) and stage 7 (0.26-0.34 μm) showed enhanced
504 peaks in several elements associated with combustion. Throughout the cruise, mass distributions of V and Ni
505 track each other well both temporally and across DRUM stages, indicative of oil combustion. Mass distributions
506 of V and Ni show higher values in the ultrafine mode between 18-19 September, indicative of an early oil
507 combustion-enriched air mass which was identified to possibly originate from Sandakan, Sabah in Borneo. Mass
508 distributions of K, Al and S show large enhancements in the fine and ultrafine modes after 27 September



coincident with a large aerosol event reported by Reid et al. (2015). In combination with the rapid spread of high AOD and NAAPS-modelled smoke concentration across the region, the strong peaks of these elements at the end of the cruise provide evidence for high levels of MC burning at the end of the cruise. Coarse-mode soil dust elements such as Fe and Si showed similarly-timed enhancements, attributed to soil particle entrainment during burning.

2. Short-term meteorological events such as TC Nesat played a key role in long-range transport as they propagated through the region, expediting the northeastward advection of aerosol emissions, an effect observed in previous studies (Atwood et al., 2012; Reid et al., 2012, 2015). The sudden variations in aerosol concentration after 24 Sept can be connected to the movement of TC Nesat through the region. Prior to these events, aerosol concentrations remained at generally low levels as NAAPS shows smoke was largely constrained to the southern hemisphere. The passage of TC Nesat advected air masses more northward, allowing them to penetrate deep enough into the northern hemisphere to be sampled by the *Vasco*. The TC's passage coincided with a shift in air mass origin from mainland Malaysia prior to 24 Sept to areas known for intense burning activity, most notably Southern Kalimantan by the end of the cruise. This corresponded to a mixed aerosol event from 24 to 26 Sept attributed to Brunei, Borneo and a significant increase in biomass burning tracer concentrations from 28 to 30 Sept attributed to Southern Kalimantan. Between these aerosol events, a clean marine event from 26 until 28 Sept was characterized by high concentrations of Cl and low levels of elements associated with anthropogenic sources. Back trajectories showed that air masses travelled through the open, central SCS/WPS which suggest nearly pure sea spray was sampled.

3. Five sources across the three modes were resolved by the PMF analysis: biomass burning, oil combustion, soil dust, sea spray, and fly ash. A threshold Pearson R coefficient of 0.0 was used to filter species included in the PMF analysis to improve the interpretability of the PMF solution. Results show that natural sources, sea spray and soil dust, were observed in only the coarse and fine modes while anthropogenic sources, biomass burning, oil combustion, and fly ash, were resolved purely in the fine and ultrafine modes. A strong correspondence between key elements seen on the PMF source profiles and groupings of these elements on the correlation matrices adds confidence to the PMF solution. The biomass burning PMF factor showed the highest percent contributions to total elemental PM mass: 34% in the fine mode, and 43% in the ultrafine mode. It is interesting to note that the contribution of the oil combustion factor increased significantly towards finer modes, 9% in the fine mode but 29% in the ultrafine mode, corroborating its anthropogenic identification. In terms of aerosol events, PMF source contributions were able to capture the most events seen in the raw elemental concentrations. Differences in the temporal variations between PMF-resolved sources suggest these sources are distinct. However, PMF did not differentiate between an early ultrafine Si spike from a distinct, subsequent spike in V



541 which demonstrates that PMF may merge events, leading to a loss in resolution as observed in other studies (Van
 542 Pinxteren et al., 2016). This, however, can be ameliorated with an in-depth, supervised analysis of the data as
 543 done in this study.

- 544 4. As stated above, spikes in oil combustion tracers V and Ni were observed on 18 Sept in the fine and ultrafine
 545 modes. HYSPLIT back trajectories suggest the origin of the air mass as Sandakan, an industrial area and port
 546 city of Sabah known for its oil depots and shipping activity located along the northeastern coast of Borneo. The
 547 spike in oil combustion suggest that a small city can cause drastic increases in tracer concentration depending on
 548 air mass trajectories. The strong presence of ultrafine mode Si from 18-19 September was also observed but the
 549 time series of Si is distinct from the time series of V and Ni, suggestive of a source distinct from oil combustion.
- 550 5. The 24 to 26 September event coincided with the arrival of TC Nesat east of Luzon (northeast of the *Vasco's*
 551 location). Enhancements of multiple key tracers for biomass burning, oil combustion and soil dust were observed,
 552 indicative of aerosols mixing within an air mass during transport. Biomass burning tracers K, S, Si, Al show
 553 enhancements over a wider period (24-26 Sept) than that of oil combustion tracers V and Ni, which spiked at the
 554 end of the period. Furthermore, aerosol-convection interactions were observed as sharp dips in the concentrations
 555 of biomass burning and soil dust tracers around 25 Sept before recovery. Interestingly, this dip was not observed
 556 for oil combustion tracers V, Ni. This cold pool event was reported in detail by Reid et al. (2015) and this study
 557 further elaborated on its impact on PM of different elemental composition. This case demonstrates the effect of
 558 short-term or high frequency phenomena on aerosol transport in the MC. HYSPLIT back trajectories show that
 559 air masses begin to travel from the southwest MC in response to TC Nesat's inflow arm. Air masses during the
 560 24-26 September event pass through Brunei, a shipping hub located along the northeastern coast of Borneo,
 561 which explains the increase in oil combustion tracers V and Ni. The coast was also observed to host a number of
 562 active fire hotspots. Land breeze may lead to the addition of burning plumes into the traveling air mass which
 563 would explain the enrichment.
- 564 6. The 28-30 September aerosol event showed an enrichment in K and S that coincided with a shift in back trajectory
 565 origin to Southern Kalimantan, which hosts a high fire hotspot density. MC burning may be characterized by an
 566 elevated K/S ratio and strong fine and ultrafine mode peaks in the mass distributions of S and K. The 28-30
 567 September event also coincided with the enhancement of soil dust elements in the coarse mode, indicative of soil
 568 particle entrainment during burning activity (Reid et al., 2015).

569 The study identified source locations of aerosol and characterized the plumes during the *Vasco* 2011 cruise; however,
 570 unanswered questions remain such as the origin of the strong ultrafine Si signal detected early in the cruise (18-19 Sept) which
 571 may be connected to a rapid local nucleation event. The source location of the PMF-resolved fly ash factor also remains
 572 unidentified due to its complicated source contribution time series and unclear elemental profile. Investigation into cloud nuclei



(CN) properties during the cruise may be done to further validate the intensity and timing of plumes. In addition to the findings of this study on the elemental PM, future research on other species collected during the 2011 and 2012 *Vasco* campaigns such as trace gases may compliment and deepen our current understanding of the aerosol environment in the SCS/WPS by adding more degrees of freedom, specifically the lifetimes of trace gases and potential for secondary aerosol formation during transport.

Author contribution

MRAH performed the analysis and prepared the manuscript. MTC supervised the analysis, especially for the PMF section. MOLC supervised the analysis and provided input for the manuscript. JSR collected the data onboard the *Vasco*, supervised the analysis, provided input for the manuscript. PX provided the NAAPS Smoke model outputs for Fig. 2 and provided input for the manuscript. JBS, NDL, SNYU collected the data onboard the *Vasco*. SC, YJZ performed the XRF analysis on the data.

Data availability

The *Vasco* ship data is available through correspondence with Jeffrey S. Reid, jeffrey.reid@nrlmry.navy.mil. MODIS AOD images were obtained from the NASA Worldview application: <https://worldview.earthdata.nasa.gov/>. HYSPLIT data is accessible through the NOAA READY website (<http://www.ready.noaa.gov>). NAAPS aerosol reanalysis data can be accessed at the US GODAE server: <http://www.usgodaes.org/>.

Competing Interests

The authors declare that they have no conflict of interest.

Acknowledgements

We acknowledge the use of imagery from the NASA Worldview application (<https://worldview.earthdata.nasa.gov/>), part of the NASA Earth Observing System Data and Information System (EOSDIS). The authors gratefully acknowledge the NOAA Air Resources Laboratory (ARL) for the provision of the HYSPLIT transport and dispersion model and/or READY website (<http://www.ready.noaa.gov>) used in this publication.

References

- Alam, K., Mukhtar, A., Shahid, I., Blaschke, T., Majid, H., Rahman, S., Khan, R. and Rahman, N.: Source apportionment and characterization of particulate matter (PM₁₀) in urban environment of Lahore, *Aerosol Air Qual. Res.*, 14(7), 1851–1861, doi:10.4209/aaqr.2014.01.0005, 2014.
- Artaxo, P. and Maenhaut, W.: Aerosol Characteristics and Sources for the Amazon Basin During the Wet Season, *J. Geophys. Res.*, 95(D10), 16971–16985, 1990.



- 602 Artaxo, P., Fernandes, E. T., Martins, J. V., Yamasoe, M. A., Maenhaut, W., Longo, K. M., Castanho, A. and Hobbs, P. V.:
 603 Large-scale aerosol source apportionment in Amazonia, *J. Geophys. Res. Atmos.*, 103(D24), 31837–31847,
 604 doi:10.1029/98jd02346, 1998.
- 605 Atwood, S. A., Reid, J. S., Kreidenweis, S. M., Cliff, S. S., Zhao, Y., Lin, N. H., Tsay, S. C., Chu, Y. C. and Westphal, D.
 606 L.: Size resolved measurements of springtime aerosol particles over the northern South China Sea, *Atmos. Environ.*, 78,
 607 134–143, doi:10.1016/j.atmosenv.2012.11.024, 2012.
- 608 Atwood, S. A., Salinas, S. V., Chew, B. N., Reid, J. S., Balasubramanian, R., Yu, L. E. and Kreidenweis, S. M.: Analysis of
 609 source regions for smoke events in Singapore for the 2009 El Nino burning season, *Atmos. Environ.*, 78, 219–230,
 610 doi:10.1016/j.atmosenv.2013.04.047, 2013.
- 611 Atwood, S. A., Reid, J. S., Kreidenweis, S. M., Blake, D. R., Jonsson, H. H., Lagrosas, N. D., Xian, P., Reid, E. A., Sessions,
 612 W. R. and Simpas, J. B.: Size-resolved aerosol and cloud condensation nuclei (CCN) properties in the remote marine
 613 South China Sea-Part 1: Observations and source classification, *Atmos. Chem. Phys.*, 17(2), 1105–1123,
 614 doi:10.5194/acp-17-1105-2017, 2017.
- 615 Baker, K. R., Simon, H. and Kelly, J. T.: Challenges to modeling “cold pool” meteorology associated with high pollution
 616 episodes, *Environ. Sci. Technol.*, 45(17), 7118–7119, doi:10.1021/es202705v, 2011.
- 617 Balasubramanian, R., Qian, W.-B., Decesari, S., Facchini, M. C. and Fuzzi, S.: Comprehensive characterization of PM 2.5
 618 aerosols in Singapore, *J. Geophys. Res.*, 108(D16), doi:10.1029/2002jd002517, 2003.
- 619 Becagli, S., Sferlazzo, D. M., Pace, G., Di Sarra, A., Bommarito, C., Calzolari, G., Ghedini, C., Lucarelli, F., Meloni, D.,
 620 Monteleone, F., Severi, M., Traversi, R. and Udisti, R.: Evidence for heavy fuel oil combustion aerosols from chemical
 621 analyses at the island of Lampedusa: A possible large role of ships emissions in the Mediterranean, *Atmos. Chem. Phys.*,
 622 12(7), 3479–3492, doi:10.5194/acp-12-3479-2012, 2012.
- 623 Boucher, O., D. Randall, P. Artaxo, C. Bretherton, G. Feingold, P. Forster, V.-M. Kerminen, Y. Kondo, H. Liao, U.
 624 Lohmann, P. Rasch, S.K. Satheesh, S. Sherwood, B. Stevens and X.Y. Zhang: Clouds and Aerosols. In: *Climate Change*
 625 *2013: The Physical Science Basis. Contribution of Working Group I to the Fifth Assessment Report of the*
 626 *Intergovernmental Panel on Climate Change [Stocker, T.F., D. Qin, G.-K. Plattner, M. Tignor, S.K. Allen, J. Boschung,*
 627 *A. Nauels, Y. Xia, V. Bex and P.M. Midgley (eds.)]. Cambridge University Press, Cambridge, United Kingdom and New*
 628 *York, NY, USA, 2013.*
- 629 Cahill, T. A., Barnes, D. E., Lawton, J. A., Miller, R., Spada, N., C. R. D. W. and Kimbrough, S.: Transition metals in
 630 coarse, fine, very fine and ultra-fine particles from an interstate highway transect near Detroit, , doi:10.1016/S0065-
 631 3454(07)37008-3, 2007.



- 632 Chan, Y. C., Christensen, E., Golding, G., King, G., Gore, W., Cohen, D. D., Stelcer, E., Simpson, R., Denison, L. and
 633 Wong, N.: Source Apportionment of Ambient Volatile Organic Compounds in Major Cities in Australia By Positive
 634 Matrix Factorisation, 42(2), 22–29, 2008.
- 635 Chang, C. P., Zhuo, W., John, M. and Ching-Hwang, L.: Annual Cycle of Southeast Asia — Maritime Continent Rainfall
 636 and the Asymmetric, J. Clim., 18, 287–301, doi:10.1175/JCLI-3257.1, 2005.
- 637 Cohen, D. D., Crawford, J., Stelcer, E. and Bac, V. T.: Long range transport of fine particle windblown soils and coal fired
 638 power station emissions into Hanoi between 2001 to 2008, Atmos. Environ., 44(31), 3761–3769,
 639 doi:10.1016/j.atmosenv.2010.06.047, 2010a.
- 640 Cohen, D. D., Crawford, J., Stelcer, E. and Bac, V. T.: Characterisation and source apportionment of fine particulate sources
 641 at Hanoi from 2001 to 2008, Atmos. Environ., 44(3), 320–328, doi:10.1016/j.atmosenv.2009.10.037, 2010b.
- 642 Davison, R. L., Natusch, D. F. S. and Wallace, J. R.: Trace Elements in Fly Ash, , 8(13) [online] Available from:
 643 <https://pubs.acs.org/doi/pdf/10.1021/es60098a003?src=recsys>, 1974.
- 644 Deonarine, A., Kolker, A. and Doughten, M.: Trace Elements in Coal Ash, Usgs, (May), 1–6,
 645 doi:10.1002/9781119199090.fmatter, 2015.
- 646 Draxler, R. R. and Hess, G. D.: An overview of the HYSPLIT_4 modelling system for trajectories, Aust. Meteorol. Mag.,
 647 47, 295–308, 1998.
- 648 Draxler, R. R.: HYSPLIT4 user's guide. NOAA Tech. Memo. ERL ARL-230, NOAA Air Resources Laboratory, Silver
 649 Spring, MD., 1999.
- 650 Duncan, B. N., Martin, R. V., Staudt, A. C., Yevich, R. and Logan, J. A.: Interannual and seasonal variability of biomass
 651 burning emissions constrained by satellite observations, J. Geophys. Res., 108(D2), doi:10.1029/2002jd002378, 2003.
- 652 Engling, G., He, J., Betha, R. and Balasubramanian, R.: Assessing the regional impact of Indonesian biomass burning
 653 emissions based on organic molecular tracers and chemical mass balance modeling, Atmos. Chem. Phys., 14(15), 8043–
 654 8054, doi:10.5194/acp-14-8043-2014, 2014.
- 655 Farao, C., Canepari, S., Perrino, C. and Harrison, R. M.: Sources of PM in an industrial area: Comparison between receptor
 656 model results and semiempirical calculations of source contributions, Aerosol Air Qual. Res., 14(6), 1558–1572,
 657 doi:10.4209/aaqr.2013.08.0281, 2014.
- 658 Field, R. D. and Shen, S. S. P.: Predictability of carbon emissions from biomass burning in Indonesia from 1997 to 2006, J.
 659 Geophys. Res. Biogeosciences, 113(4), 1–17, doi:10.1029/2008JG000694, 2008.



- 660 Fujii, Y., Tohno, S., Amil, N., Latif, M. T., Oda, M., Matsumoto, J. and Mizohata, A.: Annual variations of carbonaceous
 661 PM_{2.5} in Malaysia: Influence by Indonesian peatland fires, *Atmos. Chem. Phys. Discuss.*, 15(16), 22419–22449,
 662 doi:10.5194/acpd-15-22419-2015, 2015.
- 663 Ge, C., Wang, J. and Reid, J. S.: Mesoscale modeling of smoke transport over the Southeast Asian maritime continent:
 664 Coupling of smoke direct radiative effect below and above the low-level clouds, *Atmos. Chem. Phys.*, 14(1), 159–174,
 665 doi:10.5194/acp-14-159-2014, 2014.
- 666 Gugamsetty, B., Wei, H., Liu, C. N., Awasthi, A., Tsai, C. J., Roam, G. D., Wu, Y. C. and Chen, C. F.: Source
 667 Characterization and Apportionment of PM₁₀, PM_{2.5} and PM_{0.1} by Using Positive Matrix Factorization, *Aerosol Air*
 668 *Qual. Res.*, 12(4), 476–491, doi:10.4209/aaqr.2012.04.0084, 2012.
- 669 Han, J. S., Moon, K. J., Lee, S. J., Ryu, S. Y., Cliff, S. S., Kim, Y. J. and Yi, S. M.: Size-resolved source apportionment of
 670 ambient particles by positive matrix factorization at Gosan background site in East Asia, *Atmos. Chem. Phys.*, 6(1), 211–
 671 223, doi:10.5194/acp-6-211-2006, 2006.
- 672 Hedberg, E., Gidhagen, L. and Johansson, C.: Source contributions to PM₁₀ and arsenic concentrations in Central Chile
 673 using positive matrix factorization, *Atmos. Environ.*, 39(3), 549–561, doi:10.1016/j.atmosenv.2004.11.001, 2005.
- 674 Higgins, R. W. and Shi, W.: Intercomparison of the principal modes of interannual and intraseasonal variability of the North
 675 American Monsoon System, *J. Clim.*, 14(3), 403–417, doi:10.1175/1520-0442(2001)014<0403:IOTPMO>2.0.CO;2,
 676 2001.
- 677 Hoek, G., Krishnan, R. M., Beelen, R., Peters, A., Ostro, B., Brunekreef, B. and Kaufman, J. D.: Long-term air pollution
 678 exposure and cardio-respiratory mortality: A review, *Environ. Heal. A Glob. Access Sci. Source*, 12(1),
 679 doi:10.1186/1476-069X-12-43, 2013.
- 680 Hsu, S. C., Tsai, F., Lin, F. J., Chen, W. N., Shiah, F. K., Huang, J. C., Chan, C. Y., Chen, C. C., Liu, T. H., Chen, H. Y.,
 681 Tseng, C. M., Hung, G. W., Huang, C. H., Lin, S. H. and Huang, Y. T.: A super Asian dust storm over the East and South
 682 China Seas: Disproportionate dust deposition, *J. Geophys. Res. Atmos.*, 118(13), 7169–7181, doi:10.1002/jgrd.50405,
 683 2013.
- 684 Hyer, E. J., Reid, J. S. and Zhang, J.: An over-land aerosol optical depth data set for data assimilation by filtering, correction,
 685 and aggregation of MODIS Collection 5 optical depth retrievals, *Atmos. Meas. Tech.*, 4(3), 379–408, doi:10.5194/amt-4-
 686 379-2011, 2011.



- 687 Karanasiou, A. A., Siskos, P. A. and Eleftheriadis, K.: Assessment of source apportionment by Positive Matrix Factorization
 688 analysis on fine and coarse urban aerosol size fractions, *Atmos. Environ.*, 43(21), 3385–3395,
 689 doi:10.1016/j.atmosenv.2009.03.051, 2009.
- 690 Kecorius, S., Madueno, L., Vallar, E., Alas, H., Betito, G., Birmili, W., Cambaliza, M. O., Catipay, G., Gonzaga-Cayetano,
 691 M., Galvez, M. C., Lorenzo, G., Müller, T., Simpas, J. B., Tamayo, E. G. and Wiedensohler, A.: Aerosol particle mixing
 692 state, refractory particle number size distributions and emission factors in a polluted urban environment: Case study of
 693 Metro Manila, Philippines, *Atmos. Environ.*, 170, 169–183, doi:10.1016/j.atmosenv.2017.09.037, 2017.
- 694 Landis, M. S., Pancras, J. P., Graney, J. R., White, E. M., Edgerton, E. S., Legge, A. and Percy, K. E.: Source apportionment
 695 of ambient fine and coarse particulate matter at the Fort McKay community site, in the Athabasca Oil Sands Region,
 696 Alberta, Canada, *Sci. Total Environ.*, 584–585, 105–117, doi:10.1016/j.scitotenv.2017.01.110, 2017.
- 697 Lareau, N. P., Crosman, E., Whiteman, C. D., Horel, J. D., Hoch, S. W., Brown, W. O. J. and Horst, T. W.: The persistent
 698 cold-air pool study, *Bull. Am. Meteorol. Soc.*, 94(1), 51–63, doi:10.1175/BAMS-D-11-00255.1, 2013.
- 699 Lee, E., Chan, C. K. and Paatero, P.: Application of positive matrix factorization in source apportionment of particulate
 700 pollutants in Hong Kong, *Atmos. Environ.*, 33(19), 3201–3212, doi:10.1016/S1352-2310(99)00113-2, 1999.
- 701 Lee, S.-S., Feingold, G. and Chuang, P. Y.: Effect of Aerosol on Cloud–Environment Interactions in Trade Cumulus, J.
 702 *Atmos. Sci.*, 69(12), 3607–3632, doi:10.1175/jas-d-12-026.1, 2012.
- 703 Lestari, P. and Mauliadi, Y. D.: Source apportionment of particulate matter at urban mixed site in Indonesia using PMF,
 704 *Atmos. Environ.*, 43(10), 1760–1770, doi:10.1016/j.atmosenv.2008.12.044, 2009.
- 705 Li, T., Wang, Y., Li, W. J., Chen, J. M., Wang, T. and Wang, W. X.: Concentrations and solubility of trace elements in fine
 706 particles at a mountain site, southern China: Regional sources and cloud processing, *Atmos. Chem. Phys.*, 15(15), 8987–
 707 9002, doi:10.5194/acp-15-8987-2015, 2015.
- 708 Liao, H.-T., Chou, C. C.-K., Chow, J. C., Watson, J. G., Hopke, P. K. and Wu, C.-F.: Source and risk apportionment of
 709 selected VOCs and PM_{2.5} species using partially constrained receptor models with multiple time resolution data,
 710 *Environ. Pollut.*, 205, 121–130, doi:10.1016/j.envpol.2015.05.035, 2015.
- 711 Lin, C.-Y., Wang, Z., Chen, W.-N., Chang, S.-Y., Chou, C. C. K., Sugimoto, N. and Zhao, X.: Long-range transport of Asian
 712 dust and air pollutants to Taiwan: observed evidence and model simulation, *Atmos. Chem. Phys. Discuss.*, 6(5), 10183–
 713 10216, doi:10.5194/acpd-6-10183-2006, 2007.



- 714 Lin, Y.-C., Tsai, C.-J., Wu, Y.-C., Zhang, R., Chi, K.-H., Huang, Y.-T., Lin, S.-H. and Hsu, S.-C.: Characteristics of trace
 715 metals in traffic-derived particles in Hsuehshan Tunnel, Taiwan: size distribution, potential source, and fingerprinting
 716 metal ratio, *Atmos. Chem. Phys.*, 15(8), 4117–4130, doi:10.5194/acp-15-4117-2015, 2015.
- 717 Loo, Y. Y., Billa, L. and Singh, A.: Effect of climate change on seasonal monsoon in Asia and its impact on the variability of
 718 monsoon rainfall in Southeast Asia, *Geosci. Front.*, 6(6), 817–823, doi:10.1016/j.gsf.2014.02.009, 2015.
- 719 Lynch, P., Reid, J. S., Westphal, D. L., Zhang, J., Hogan, T. F., Hyer, E. J., Curtis, C. A., Hegg, D. A., Shi, Y., Campbell, J.
 720 R., Rubin, J. I., Sessions, W. R., Turk, F. J. and Walker, A. L.: An 11-year global gridded aerosol optical thickness
 721 reanalysis (v1.0) for atmospheric and climate sciences, *Geosci. Model Dev.*, 9(4), 1489–1522, doi:10.5194/gmd-9-1489-
 722 2016, 2016.
- 723 Maloney, E. D. and Hartmann, D. L.: The Madden–Julian Oscillation, Barotropic Dynamics, and North Pacific Tropical
 724 Cyclone Formation. Part I: Observations, *J. Atmos. Sci.*, 58(17), 2545–2558, doi:10.1175/1520-
 725 0469(2001)058<2545:TMJOB>2.0.CO;2, 2001.
- 726 Mazzei, F., D’Alessandro, A., Lucarelli, F., Nava, S., Prati, P., Valli, G. and Vecchi, R.: Characterization of particulate
 727 matter sources in an urban environment, *Sci. Total Environ.*, 401(1–3), 81–89, doi:10.1016/j.scitotenv.2008.03.008,
 728 2008.
- 729 Markowski, G. R. and Filby, R.: Trace Element Concentration as a Function of Particle Size in Fly Ash from a Pulverized
 730 Coal Utility Boiler, *Environ. Sci. Technol.*, 19(9), 796–804, doi:10.1021/es00139a005, 1985.
- 731 Nakajima, T., Yoon, S. C., Ramanathan, V., Shi, G. Y., Takemura, T., Higurashi, A., Takamura, T., Aoki, K., Sohn, B. J.,
 732 Kim, S. W., Tsuruta, H., Sugimoto, N., Shimizu, A., Tanimoto, H., Sawa, Y., Lin, N. H., Lee, C. Te, Goto, D. and
 733 Schutgens, N.: Overview of the Atmospheric Brown Cloud East Asian Regional Experiment 2005 and a study of the
 734 aerosol direct radiative forcing in east Asia, *J. Geophys. Res. Atmos.*, 112(24), 1–23, doi:10.1029/2007JD009009, 2007.
- 735 Nigam, A., Welch, W., Wayne Miller, J., and Cocher III, D. R.: Effect of fuel sulphur content and control technology on PM
 736 emission from ship’s auxiliary engine. Proceeding international aerosol conference, St. Paul, USA, 10–15 September
 737 2006, 1531–1532, 2006.
- 738 Oanh, Nguyen Thi Kim. Integrated air quality management: Asian case studies. Boca Raton, FL: Taylor & Francis, 2013.
 739 Print.
- 740 O’Sullivan, D. Murray, B. J., Malkin, T. L., Whale, T. F., Umo, N. S., Atkinson, J. D., Price, H. C., Baustian, K. J., Browse,
 741 J. and Webb, M. E.: Ice nucleation by fertile soil dusts: relative importance of mineral and biogenic components, *Atmos.*
 742 *Chem. Phys.*, 14(4), 1853–1867, doi:10.5194/acp-14-1853-2014, 2014.



- 743 Paatero, P. and Tapper, U.: Positive matrix factorization: A non-negative factor model with optimal utilization of error
 744 estimates of data values, *Environmetrics*, 5(2), 111–126, doi:10.1002/env.3170050203, 1994.
- 745 Paatero, P. and Hopke, P. K.: Discarding or downweighting high-noise variables in factor analytic models, *Anal. Chim.*
 746 *Acta*, 490(1–2), 277–289, doi:10.1016/S0003-2670(02)01643-4, 2003.
- 747 Paterson, K. G., Sagady, J. L., Hooper, D. L., Bertman, S. B., Carroll, M. A. and Shepson, P. B.: Analysis of air quality data
 748 using positive matrix factorization, *Environ. Sci. Technol.*, 33(4), 635–641, doi:10.1021/es980605j, 1999.
- 749 Polissar, A. V., Hopke, P. K., Paatero, P., Malm, W. C. and Sisler, J. F.: Atmospheric aerosol over Alaska 2. Elemental
 750 composition and sources, *J. Geophys. Res. Atmos.*, 103(D15), 19045–19057, doi:10.1029/98JD01212, 1998.
- 751 Prospero, J. M.: Long-range transport of mineral dust in the global atmosphere: Impact of African dust on the environment
 752 of the southeastern United States, *Proc. Natl. Acad. Sci.*, 96(7), 3396–3403, doi:10.1073/pnas.96.7.3396, 1999.
- 753 Qi, L., Chen, M., Ge, X., Zhang, Y. and Guo, B.: Seasonal variations and sources of 17 aerosol metal elements in suburban
 754 Nanjing, China, *Atmosphere (Basel)*, 7(12), 1–21, doi:10.3390/atmos7120153, 2016.
- 755 Qian, J.-H., Robertson, A. W. and Moron, V.: Interactions among ENSO, the Monsoon, and Diurnal Cycle in Rainfall
 756 Variability over Java, Indonesia, *J. Atmos. Sci.*, 67(11), 3509–3524, doi:10.1175/2010jas3348.1, 2010.
- 757 Querol, X., Viana, M., Alastuey, A., Amato, F., Moreno, T., Castillo, S., Pey, J., Rosa, J. de la, Campa, A. S. de la, Artinano,
 758 B., Salvador, P., Santos, S. G. Dos, Fernandez-Patier, R., Moreno-Grau, S., Negral, L., Minguillon, M. C., Monfort, E.,
 759 Gil, J. I., Inza, A., Ortega, L. A., Santamaria, J. M. and Zabalza, J.: Source origin of trace elements in PM from regional
 760 background, urban and industrial sites of Spain, *Atmos. Environ.*, 41(34), 7219–7231,
 761 doi:10.1016/j.atmosenv.2007.05.022, 2007.
- 762 Raabe, O. G., Braaten, D. A., Axelbaum, R. L., Teague, S. V and Cahill, T. A.: Calibration studies of the drum impactor, *J.*
 763 *Aerosol Sci.*, 19(2), 183–195, doi:10.1016/0021-8502(88)90222-4, 1988.
- 764 Reid, J. S., Flocchini, R. G., Cahill, T. A., Ruth, R. S. and Salgado, D. P.: Local meteorological, transport, and source
 765 aerosol characteristics of late autumn Owens Lake (dry) dust storms, *Atmos. Environ.*, 28(9), 1699–1706,
 766 doi:10.1016/1352-2310(94)90315-8, 1994.
- 767 Reid, J. S., Hyer, E. J., Prins, E. M., Westphal, D. L., Zhang, J., Wang, J., Christopher, S. A., Curtis, C. A., Schmidt, C. C.,
 768 Eleuterio, D. P., Richardson, K. A. and Hoffman, J. P.: Global monitoring and forecasting of biomass-burning smoke:
 769 Description of and lessons from the fire Locating and Modeling of Burning Emissions (FLAMBE) program, *IEEE J. Sel.*
 770 *Top. Appl. Earth Obs. Remote Sens.*, 2(3), 144–162, doi:10.1109/JSTARS.2009.2027443, 2009.



- 771 Reid, J. S., Xian, P., Hyer, E. J., Flatau, M. K., Ramirez, E. M., Turk, F. J., Sampson, C. R., Zhang, C., Fukada, E. M. and
 772 Maloney, E. D.: Multi-scale meteorological conceptual analysis of observed active fire hotspot activity and smoke optical
 773 depth in the Maritime Continent, *Atmos. Chem. Phys.*, 12(4), 2117–2147, doi:10.5194/acp-12-2117-2012, 2012.
- 774 Reid, J., Hyer, E., Johnson, R., Holben, B. N., Yokelson, R., Zhang, J., Campbell, J., Christopher, S., DiGirolamo, L., Giglio,
 775 L., Holz, R., Kearney, C., Miettinen, J., Reid, E., Turk, F. J., Wang, J., Xian, P., Zhao, G., Balasubramanian, R., Chew,
 776 B. N., Janjai, S., Lagrosas, N., Lestari, P., Lin, N.-H., Mahmud, M., Nguyen, A. X., Norris, B., Oanth, N. T. K., Oo, M.,
 777 Salinas, S. V., Welton, E. J. and Liew, S. C.: Observing and understanding the Southeast Asian aerosol system by remote
 778 sensing: An initial review and analysis for the Seven Southeast Asian Studies (7SEAS) program, *Atmos. Res.*, 122, 403–
 779 468, doi:10.1016/j.atmosres.2012.06.005, 2013.
- 780 Reid, J. S., Lagrosas, N. D., Jonsson, H. H., Reid, E. A., Sessions, W. R., Simpas, J. B., Uy, S. N., Boyd, T. J., Atwood, S.
 781 A., Blake, D. R., Campbell, J. R., Cliff, S. S., Holben, B. N., Holz, R. E., Hyer, E. J., Lynch, P., Meinardi, S., Posselt, D.
 782 J., Richardson, K. A., Salinas, S. V., Smirnov, A., Wang, Q., Yu, L. and Zhang, J.: Observations of the temporal
 783 variability in aerosol properties and their relationships to meteorology in the summer monsoonal South China Sea/East
 784 Sea: the scale-dependent role of monsoonal flows, the Madden–Julian Oscillation, tropical cyclones, squall lines and cold
 785 pools, *Atmos. Chem. Phys.*, 15(4), 1745–1768, doi:10.5194/acp-15-1745-2015, 2015.
- 786 Reid, J. S., Xian, P., Holben, B. N., Hyer, E. J., Reid, E. A., Salinas, S. V., Zhang, J., Campbell, J. R., Chew, B. N., Holz, R.
 787 E., Kuciauskas, A. P., Lagrosas, N., Posselt, D. J., Sampson, C. R., Walker, A. L., Welton, E. J. and Zhang, C.: Aerosol
 788 meteorology of the Maritime Continent for the 2012 7SEAS southwest monsoon intensive study – Part 1: regional-scale
 789 phenomena, *Atmos. Chem. Phys.*, 16(22), 14041–14056, doi:10.5194/acp-16-14041-2016, 2016.
- 790 Ross, A. D., Holz, R. E., Quinn, G., Reid, J. S., Xian, P., Turk, F. J. and Posselt, D. J.: Exploring the First Aerosol Indirect
 791 Effect over the Maritime Continent Using a Ten-Year Collocated MODIS, CALIOP, and Model Dataset, *Atmos. Chem.*
 792 *Phys. Discuss.*, (March), 1–28, doi:10.5194/acp-2018-4, 2018.
- 793 Rolph, G., Stein, A., and Stunder, B. Real-time Environmental Applications and Display sYstem: READY. *Environmental*
 794 *Modelling & Software*, 95, 210–228, https://doi.org/10.1016/j.envsoft.2017.06. 2017.
- 795 Santoso, M., Lestiani, D. D., Mukhtar, R., Hamonangan, E., Syafrul, H., Markwitz, A. and Hopke, P. K.: Preliminary study
 796 of the sources of ambient air pollution in Serpong, Indonesia, *Atmos. Pollut. Res.*, 2(2), 190–196,
 797 doi:10.5094/apr.2011.024, 2011.
- 798 Schlosser, J. S., Braun, R. A., Bradley, T., Dadashazar, H., MacDonald, A. B., Aldhaif, A. A., Aghdam, M. A., Mardi, A. H.,
 799 Xian, P. and Sorooshian, A.: Analysis of aerosol composition data for western United States wildfires between 2005 and



- 800 2015: Dust emissions, chloride depletion, and most enhanced aerosol constituents, *J. Geophys. Res. Atmos.*, 122(16),
 801 8951–8966, doi:10.1002/2017JD026547, 2017.
- 802 Seneviratne, M. C. S., Waduge, V. A., Hadagiripathira, L., Sanjeevani, S., Attanayake, T., Jayaratne, N. and Hopke, P. K.:
 803 Characterization and source apportionment of particulate pollution in Colombo, Sri Lanka, *Atmos. Pollut. Res.*, 2(2),
 804 207–212, doi:10.5094/apr.2011.026, 2011.
- 805 Shi, Y., Zhang, J., Reid, J. S., Liu, B., and Hyer, E. J.: Critical evaluation of cloud contamination in the MISR aerosol
 806 products using MODIS cloud mask products, *Atmos. Meas. Tech.*, 7, 1791–1801, 2014.
- 807 Song, Y., Xie, S., Zhang, Y., Zeng, L., Salmon, L. G. and Zheng, M.: Source apportionment of PM_{2.5} in Beijing using
 808 principal component analysis/absolute principal component scores and UNMIX, *Sci. Total Environ.*, 372(1), 278–286,
 809 doi:10.1016/j.scitotenv.2006.08.041, 2006.
- 810 Sorooshian, A., Feingold, G., Lebsock, M. D., Jiang, H., and Stephens, G. L.: On the precipitation susceptibility of clouds to
 811 aerosol perturbations, *Geophys. Res. Lett.*, 36, L13803, doi:10.1029/2009GL038993, 2009.
- 812 Sowlat, M. H., Hasheminassab, S. and Sioutas, C.: Source apportionment of ambient particle number concentrations in
 813 central Los Angeles using positive matrix factorization (PMF), *Atmos. Chem. Phys.*, 16(8), 4849–4866, doi:10.5194/acp-
 814 16-4849-2016, 2016.
- 815 Stein, A.F., Draxler, R.R., Rolph, G.D., Stunder, B.J.B., Cohen, M.D., and Ngan, F. NOAA's HYSPLIT atmospheric
 816 transport and dispersion modeling system, *Bull. Amer. Meteor. Soc.*, 96, 2059–2077, [http://dx.doi.org/10.1175/BAMS-D-](http://dx.doi.org/10.1175/BAMS-D-14-00110.1)
 817 [14-00110.1](http://dx.doi.org/10.1175/BAMS-D-14-00110.1), 2015.
- 818 Thurston, G. D., Ito, K. and Lall, R.: A Source Apportionment of U.S. Fine Particulate Matter Air Pollution, *Atmos.*
 819 *Environ.*, 45(24), 3831–3840, doi: 10.1016/j.atmosenv.2011.04.070, 1994.
- 820 Tian, S. L., Pan, Y. P. and Wang, Y. S.: Size-resolved source apportionment of particulate matter in urban Beijing during
 821 haze and non-haze episodes, *Atmos. Chem. Phys.*, 16(1), 1–19, doi:10.5194/acp-16-1-2016, 2016.
- 822 Van Pinxteren, D., Fomba, K. W., Spindler, G., Müller, K., Poulain, L., Iinuma, Y., Löschau, G., Hausmann, A. and
 823 Herrmann, H.: Regional air quality in Leipzig, Germany: Detailed source apportionment of size-resolved aerosol
 824 particles and comparison with the year 2000, *Faraday Discuss.*, 189, 291–315, doi:10.1039/c5fd00228a, 2016.
- 825 Viana, M., Kuhlbusch, T. A. J., Querol, X., Alastuey, A., Harrison, R. M., Hopke, P. K., Winiwarter, W., Vallius, M., Szidat,
 826 S., Prévôt, A. S. H., Hueglin, C., Bloemen, H., Wählin, P., Vecchi, R., Miranda, A. I., Kasper-Giebl, A., Maenhaut, W.
 827 and Hitenberger, R.: Source apportionment of particulate matter in Europe: A review of methods and results, *J. Aerosol*
 828 *Sci.*, 39(10), 827–849, doi:10.1016/j.jaerosci.2008.05.007, 2008.



- 829 Visser, S., Slowik, J. G., Furger, M., Zotter, P., Bukowiecki, N., Canonaco, F., Flechsig, U., Appel, K., Green, D. C.,
 830 Tremper, A. H., Young, D. E., Williams, P. I., Allan, J. D., Coe, H., Williams, L. R., Mohr, C., Xu, L., Ng, N. L.,
 831 Nemitz, E., Barlow, J. F., Halios, C. H., Fleming, Z. L., Baltensperger, U. and Prévôt, A. S. H.: Advanced source
 832 apportionment of size-resolved trace elements at multiple sites in London during winter, *Atmos. Chem. Phys.*, 15(19),
 833 11291–11309, doi:10.5194/acp-15-11291-2015, 2015.
- 834 Wang, B., Wu, R. and Fu, X.: Pacific–East Asian Teleconnection: How Does ENSO Affect East Asian Climate?, *J. Clim.*,
 835 13(9), 1517–1536, doi:10.1175/1520-0442(2000)013<1517:PEATHD>2.0.CO;2, 2000.
- 836 Wang, S.-H., Tsay, S.-C., Lin, N.-H., Hsu, N. C., Bell, S. W., Li, C., Ji, Q., Jeong, M.-J., Hansell, R. A., Welton, E. J.,
 837 Holben, B. N., Sheu, G.-R., Chu, Y.-C., Chang, S.-C., Liu, J.-J. and Chiang, W.-L.: First detailed observations of long-
 838 range transported dust over the northern South China Sea, *Atmos. Environ.*, 45(27), 4804–4808,
 839 doi:10.1016/j.atmosenv.2011.04.077, 2011.
- 840 Wang, Z., Sorooshian, A., Prabhakar, G., Coggon, M. M. and Jonsson, H. H.: Impact of emissions from shipping, land, and
 841 the ocean on stratocumulus cloud water elemental composition during the 2011 E-PEACE field campaign, *Atmos.*
 842 *Environ.*, 89, 570–580, doi:10.1016/j.atmosenv.2014.01.020, 2014.
- 843 Webster, P. J., Magana, V. O., Palmer, T. N., Shukla, J., Tomas, R. A., Yanai, M. and Yasunari, T.: Monsoons : Processes ,
 844 predictability , and the prospects for prediction 2 . Description of the Monsoons, *Weather*, 103(C7), 14451–14510, 1998.
- 845 Weichenthal, S., Villeneuve, P. J., Burnett, R. T., Donkelaar, A. van, Martin, R. V., Jones, R. R., DellaValle, C. T., Sandler,
 846 D. P., Ward, M. H. and Hoppin, J. A.: Long-Term Exposure to Fine Particulate Matter: Association with Nonaccidental
 847 and Cardiovascular Mortality in the Agricultural Health Study Cohort, *Environ. Health Perspect.*, 122(6), 609–615,
 848 doi:10.1289/ehp.1307277, 2014.
- 849 Wimolwattanapun, W., Hopke, P. K. and Pongkiatkul, P.: Source apportionment and potential source locations of PM_{2.5} and
 850 PM_{2.5}–10 at residential sites in metropolitan Bangkok, *Atmos. Pollut. Res.*, 2(2), 172–181, doi:10.5094/apr.2011.022,
 851 2011.
- 852 Witt, M., Baker, A. R. and Jickells, T. D.: Atmospheric trace metals over the Atlantic and South Indian Oceans:
 853 Investigation of metal concentrations and lead isotope ratios in coastal and remote marine aerosols, *Atmos. Environ.*,
 854 40(28), 5435–5451, doi:10.1016/j.atmosenv.2006.04.041, 2006.
- 855 Wu, C., Larson, T. V., Wu, S., Williamson, J., Westberg, H. H. and Liu, L.-J. S.: Source apportionment of PM_{2.5} and
 856 selected hazardous air pollutants in Seattle, *Sci. Total Environ.*, 386(1–3), 42–52, doi:10.1016/j.scitotenv.2007.07.042,
 857 2007.



- 858 Xian, P., Reid, J. S., Atwood, S. A., Johnson, R. S., Hyer, E. J., Westphal, D. L. and Sessions, W.: Smoke aerosol transport
 859 patterns over the Maritime Continent, *Atmos. Res.*, 122, 469–485, doi:10.1016/j.atmosres.2012.05.006, 2013.
- 860 Xie, R. K., Seip, H. M., Liu, L. and Zhang, D. S.: Characterization of individual airborne particles in Taiyuan City, China,
 861 *Air Qual. Atmos. Heal.*, 2(3), 123–131, doi:10.1007/s11869-009-0039-x, 2009.
- 862 Xing, Y. F., Xu, Y. H., Shi, M. H. and Lian, Y. X.: The impact of PM_{2.5} on the human respiratory system, *J. Thorac. Dis.*,
 863 8(1), E69–E74, doi:10.3978/j.issn.2072-1439.2016.01.19, 2016.
- 864 Yuan, B., Shao, M., Gouw, J. de, Parrish, D. D., Lu, S., Wang, M., Zeng, L., Zhang, Q., Song, Y., Zhang, J. and Hu, M.:
 865 Volatile organic compounds (VOCs) in urban air: How chemistry affects the interpretation of positive matrix
 866 factorization (PMF) analysis, *J. Geophys. Res. Atmos.*, 117(D24), 1–17, doi:10.1029/2012jd018236, 2012.
- 867 Yusuf, A. A. and Francisco, H.: Climate change vulnerability mapping for Southeast Asia, *Economy and Environment*
 868 *Program for Southeast Asia (EEPSEA)* report, available at: <http://www.eepsea.net> (last access: July 2014), 32 pp., 2009.
- 869 Zhang, C.: Madden-Julian Oscillation, *Rev. Geophys.*, 43, RG2003, doi:10.1029/2004RG000158, 2005.
- 870 Zhang, J. and Reid, J. S.: MODIS Aerosol Product Analysis for Data Assimilation: Assessment of Level 2 Aerosol Optical
 871 Thickness Retrievals, *J. Geophys. Res.-Atmos.*, 111, 22207, doi:10.1029/2005JD006898, 2006.
- 872 Zheng, C., Zhao, C., Zhu, Y., Wang, Y., Shi, X., Wu, X., Chen, T., Wu, F. and Qiu, Y.: Analysis of influential factors for the
 873 relationship between PM_{2.5} and AOD in Beijing, *Atmos. Chem. Phys.*, 17(21), 13473–13489, doi:10.5194/acp-17-
 874 13473-2017, 2017.
- 875 Zivanovic, V.: XRF analysis of mineralogical matrix effects and differences between pulverized and fused ferromanganese
 876 slag, *Chem. Ind. Chem. Eng. Q.*, 17(2), 231–237, doi:10.2298/ciceq101104008z, 2011.



877 **Table 1. PM_{1.5}/PM₁₀ ratio slopes for elements ordered by ratio-slope.**

	<i>Ratio slope</i>	<i>R-squared correlation</i>	<i>Ratio average</i>	<i>Standard deviation</i>
V	0.94	0.99	0.95	0.07
K	0.82	0.94	0.35	0.21
S	0.8	0.92	0.49	0.17
Zn	0.74	0.94	0.62	0.04
Y	0.7	0.7	0.53	0.11
Zr	0.7	0.63	0.65	0.07
Mo	0.7	0.67	0.65	0.04
Ti	0.68	0.7	0.53	0.08
Rb	0.61	0.64	0.73	0.09
Al	0.51	0.68	0.55	0.12
Pb	0.47	0.44	0.67	0.06
Cu	0.4	0.42	0.63	0.05
Ni	0.31	0.33	0.61	0.08
As	0.31	0.36	0.33	0.26
Mn	0.3	0.62	0.49	0.19
Si	0.29	0.56	0.32	0.13
Se	0.2	0.24	0.59	0.06
P	0.19	0.32	0.27	0.08
Na	0.16	0.57	0.17	0.03
Sr	0.16	0.11	0.49	0.08
Br	0.13	0.17	0.47	0.08
Ca	0.07	0.59	0.1	0.05
Cl	0.06	0.67	0.04	0.02
Fe	0.06	0.38	0.24	0.12
Mg	0.03	0.29	0.07	0.03
Co	0.03	0.03	0.57	0.1
Ga	0.03	0.04	0.56	0.09
Cr	0.01	0.02	0.19	0.19

878



879 **Table 2. Sources identified in each size range with PMF. Coarse (1.15-10 μm), fine (0.34-1.15 μm) and ultrafine (0.07-**
 880 **0.34 μm).**

Source	Major Components	Coarse	Fine	Ultrafine
Biomass Burning	K, S, Si, Al, As		+	+
Oil Combustion	V		+	+
Sea Spray	Cl, Mg, P, Br	+	+	
Soil Dust	Fe, Al, Si, Ca, Ti, Zn	+	+	
Fly ash	As, Se, Pb, Zn, Ti		+	+

881

882